Chitosan/dialdehyde cellulose hydrogels with covalently anchored polypyrrole: Novel conductive, antibacterial, antioxidant, immunomodulatory, and anti-inflammatory materials

Chitosan/dialdehyde cellulose hydrogels with covalently anchored polypyrrole: novel conductive, antibacterial, antioxidant, immunomodulatory, and anti-inflammatory materials

Simona Káčerová,[1] Monika Muchová,[1] Hana Doudová,[1] Lukáš Münster,[1] Barbora Hanulíková,[1] Kristýna Valášková[1], Věra Kašpárková[1,3], Ivo Kuřitka,[1] Petr Humpolíček,[1,3] Zdenka Víchová,[1] Ondřej Vašíček,[2*] Jan Vícha[1*]*

[1]Centre of Polymer Systems, Tomas Bata University in Zlín, tř. Tomáše Bati 5678, 760 01 Zlín, Czech Republic

[2]Institute of Biophysics of the Czech Academy of Sciences, Kralovopolská 135, 612 00 Brno, Czech Republic

[3] Department of Fat, Surfactant and Cosmetics Technology, Faculty of Technology, Tomas Bata University in Zlín, nám. T. G. Masaryka 5555, 760 01 Zlín, Czech Republic

Emails: jvicha@utb.cz, capakova@utb.cz, ondrej.vasicek@ibp.cz

Abstract:

In this work, conductive composite hydrogels with covalently attached polypyrrole (PPy) nanoparticles are prepared. Hydrogels are based on partially re-acetylated chitosan soluble at physiological pH without any artificial structural modifications or need for an acidic environment, which simplifies synthesis and purification. Low-toxic and sustainable dialdehyde cellulose (DAC) was used for crosslinking chitosan and covalent anchoring of PPy colloidal particles. The condensation reaction between DAC and PPy is reported for the first time and improves not only the anchoring of PPy particles but also control over the properties of the final composite. The soluble chitosan and PPy particles are shown to act in synergy, which improves the biological properties of the materials. Prepared composite hydrogels are non-cytotoxic, non-irritating, antibacterial, can capture reactive oxygen species often related to excessive inflammation, have conductivity similar to human tissues, enhance *in vitro* cell growth (migration assay), and have immunomodulatory effects related to the stimulation of neutrophils and macrophages. The covalent attachment of PPy also strengthens the hydrogel network. The aldol condensation as a method for PPy covalent anchoring thus presents an interesting possibility for the development of advanced biomaterials in the future.

Keywords: wound healing; dialdehyde cellulose; chitosan; polypyrrole; hydrogel;

1. Introduction

Skin is the largest organ of the body and forms the first line of defense against the environment. A skin wound, defined as any damage or disorder in the healthy structure and function of the skin, (MacNeil, 2007) may provide serious health risks. Although skin has a great capacity for healing, dermal wound repair is a complex dynamic process that can be disturbed by various factors. It is composed of several stages. (Moeini et al., 2020) The first is hemostasis, in which blood clots at the wounded site. The second stage is the inflammatory phase, during which proteolytic enzymes and pro-inflammatory cytokines are released in the wound zone, causing the generation of reactive oxygen species (ROS) by inflammatory cells. While ROS in low concentrations protects the organism from bacteria and has a positive impact on wound healing, in higher concentrations they become detrimental and could cause lipid peroxidation and severe cell damage, further increasing oxidative stresses and leading to the development of chronic wounds. (Bryan et al., 2012) In the same phase of wound healing, the foreign contaminants are also removed from the wound by neutrophils and macrophages, while the wound is kept moist and clean by wound exudate which further supports the healing process. Next is a proliferation stage during which the granulation tissue and extracellular matrix are formed. These are then remodeled in the fourth stage of the healing process, resulting in the formation of new tissue. (Das & Baker, 2016)

While traditional wound dressings are usually applied to stop bleeding and protect the wound from the surrounding environment, they do little to promote wound healing, prevent infection, or reduce excessive inflammation. This has led to the development of "active" wound dressings, which are designed to support all the phases of wound healing, keep the wound moist, absorb excessive exudate, reduce inflammation, accelerate wound healing, provide antibacterial action, and prevent infection by shielding the wound from contamination and pathogens.(Ali Khan et al., 2020) Simultaneously, the wound dressing should be biocompatible, elastic, and adhesive to easily move with the skin, but also easy to remove. Both synthetic and natural polymers and their combinations have been used for the preparation of such materials.(Das & Baker, 2016) Hydrogels in particular are promising wound dressings due to their 3D interconnected structure, high water content, and mechanical properties similar to soft tissues. They are also excellent in maintaining a humid wound environment, accepting the exudate, cooling and soothing the wound, and allowing the oxygen and water vapor to pass through. (W. Feng & Wang, 2023) They can be composed of biologically active molecules and also accommodate a variety of drugs or particles providing additional therapeutic effects, and their structure and biological effects can be engineered by using advanced techniques such as *in situ* molding or 3D printing. (Norahan et al., 2022)

Chitosan, a linear polysaccharide with N-acetyl-glucosamine and N-glucosamine units linked by β-(1–4) glycosidic bonds, is one of the most promising candidates for wound treatment materials due to its biocompatibility, biodegradability, low toxicity, antimicrobial, antioxidant, analgesic, and hemostatic properties. (Bano et al., 2017) Various wound management systems and dressings based on chitosan, its derivatives, grafts, blends, and composites in the form of powders, particles, sponges, membranes, or (hydro)gels have been prepared, see the reviews dedicated to this topic. (Ali Khan et al., 2020; Bano et al., 2017; Matica et al., 2019; Moeini et al., 2020; Patrulea et al., 2015) Regarding the most recent research, Feng et al. discuss various mechanisms of chitosan-based functional materials for skin wound repair, from hemostatic to antibacterial properties, and also covers various smart, self-healing, bioactive and composite chitosan hydrogels. (P. Feng et al., 2021) Benefits of chitosan functionalization and its combination with various nano-sized materials into advanced composites designed for wound healing are reviewed by Biswal et al. (Biswal et al., 2023) The hemostatic properties of chitosan and its various derivatives have been also been recently reviewed in detail, the mechanism of action discussed, and the effects of deacetylation degree,

molecular weight, and chemical modification on the hemostatic performance of chitosan hydrogels summarized. (Fan et al., 2023) All these work indicate that chitosan-based wound helaing materials are dynamically developing field with considerable potential.

However, the majority of positive effects of chitosan are associated with its cationic nature in an acidic environment, as abundant $–NH_2$ groups in its structure become protonated when the pH is lower than its pK_a value of ~6.5. (Wang et al., 2006) The positive charge of $–NH_3^+$ groups allows chitosan to dissolve in acidic aqueous solutions and electrostatically interact with microbial membranes, disrupting them or forming an impervious layer blocking the flow of nutrients and oxygen into the bacterial cell. (Matica et al., 2019) As chitosan loses its charge at physiological pH (above pK_a), it becomes insoluble and its antimicrobial activity essentially vanishes, as recently summarized by Matica et al. (Matica et al., 2019) The insolubility and loss of antimicrobial activity under physiological conditions are major limitations for applications of chitosan-based systems. Water-soluble chitosan derivatives, such as trimethyl chitosan, carboxymethyl chitosan, or carboxymethyl-trimethyl-chitosan were developed to counter these issues. (Patrulea et al., 2015) Various strategies and chemical modifications for the preparation of water-soluble chitosan derivatives, their biological activities, and possible applications have been recently discussed by Yusof et al. (Wan Yusof et al., 2023) Such modifications, however, generally introduce artificial functional groups to the chitosan structure.

The synthesis of water-soluble half N-acetylated chitosan (SCN, Soluble Chitosan) provides a possible solution. (T. Feng et al., 2006; Kubota et al., 2000; Qin et al., 2006) While commercially available chitosans usually have a degree of deacetylation (DD) above 75%, SCN is prepared by partial re-acetylation of chitosan to DD ~50%, at which point it became soluble at physiological pH in contrast to chitosan with both higher and lower DD. This is caused by different inter-strand distances in chitosan and chitin, which are held together by hydrogen bonds involving amino groups (chitosan) or N-acetate groups (chitin). While single binding mode prevails in chitosan and solubility-limiting crystallites are formed, randomly distributed amino and N-acetate groups of SCN result in significantly lower crystallinity which improves its solubility.(Sogias et al., 2010) Compared to other soluble chitosan derivatives, acetylation of chitosan is a completely natural modification that only alters its DD without introducing artificial functional groups. Although known for quite some time, (T. Feng et al., 2006; Kubota et al., 2000; Qin et al., 2006) the SCN is rather underutilized in the field of wound dressing materials compared to other soluble chitosan derivatives (Patrulea et al., 2015). One of the possible reasons may be its comparatively lower antimicrobial properties under acidic conditions compared to highly deacetylated chitosan, despite SCN having the highest affinity for *E. coli* from all tested samples. (Qin et al., 2006) This is likely caused by limited adsorption to bacterial membranes given by alternating amino and N-acetate groups. This is however not relevant for applications under physiological conditions where chitosan with high DD is insoluble.

The development of wound dressings is clearly a challenging task. Many hurdles need to be overcome, ranging from the material design on a (macro)molecular level to the battery of biological tests. In this contribution, we focus on the former by developing composite polypyrrole-containing hydrogels, which are rationally designed to strengthen the natural characteristics of SCN, mitigate its drawbacks, and provide further benefits without using toxic crosslinkers, modifications, or substances. In other words, we seek to improve the current design of conductive composite hydrogels to provide a background for the possible future development which could lead to advanced wound healing materials.

The novelty of our approach is based on the synergy of the immunostimulatory action of polypyrrole colloidal particles (PPy), and the new method for their covalent tethering and localization. The introduction of PPy particles also provides conductivity under physiological conditions. For a recent comprehensive

review discussing the effects, advantages, and recent development of conductive biomaterials for wound healing and skin tissue engineering, see the recent work of Yu et al. (Yu et al., 2021) Although PPy does not provide such a high conductivity as other non-metallic conductors such as graphene oxide, which is currently investigated as a component of hydrogels for wound healing and wearables (W. Feng & Wang, 2022; Jin et al., 2020), it provides additional antioxidative, antibacterial, and immunostimulatory properties, (Káčerová et al., 2023) all of which are highly beneficial and complement properties of SCN. However, as neat unsupported PPy colloids are unsuitable for wound dressings due to the risk of particle leaching into the wound, the 2,3-dialdehyde cellulose (DAC) is used to not only crosslink the SCN but also covalently anchor the pre-formed PPy in an elegant approach employing two different chemistries of a single molecule, see Scheme 1. The DAC is a cellulose derivative prepared by regioselective oxidation of hydroxyl groups at C2 and C3 of the anhydroglucose unit by $NaIO_4$ (Kim et al., 2000) introducing a pair of reactive –CHO groups into each oxidized unit. Compared to highly toxic organic dialdehydes, e.g. glutaraldehyde, (Abdelgawad et al., 2014) the DAC has significantly lower toxicity (Muchová et al., 2022) and is considered sustainable and green material. (Ding & Wu, 2020) Besides, its macromolecular character allows it to react with numerous (macro)molecules at once, which greatly improves the crosslinking effectiveness, particularly at low concentrations. (Muchová et al., 2020, 2022; Münster et al., 2019) While the reaction between DAC and SCN involves a well-known Schiff base formation, (Důbravová et al., 2024; Kim et al., 2017) the reaction between DAC and PPy is described for the first time.

Last but not least, the employed approach provides excellent control over the amount and form of PPy in the hydrogels, as the desired amount of pre-synthesized PPy particles with optimized properties (size, polydispersity) can be homogeneously blended and anchored in hydrogel network. This is a significant improvement over other methods relying on coating, dip-coating, or poorly controllable *in situ* PPy polymerization, often leading to the formation of local PPy deposits and clusters. (Korupalli et al., 2021; Y. Liang & Goh, 2020; Yu et al., 2021)

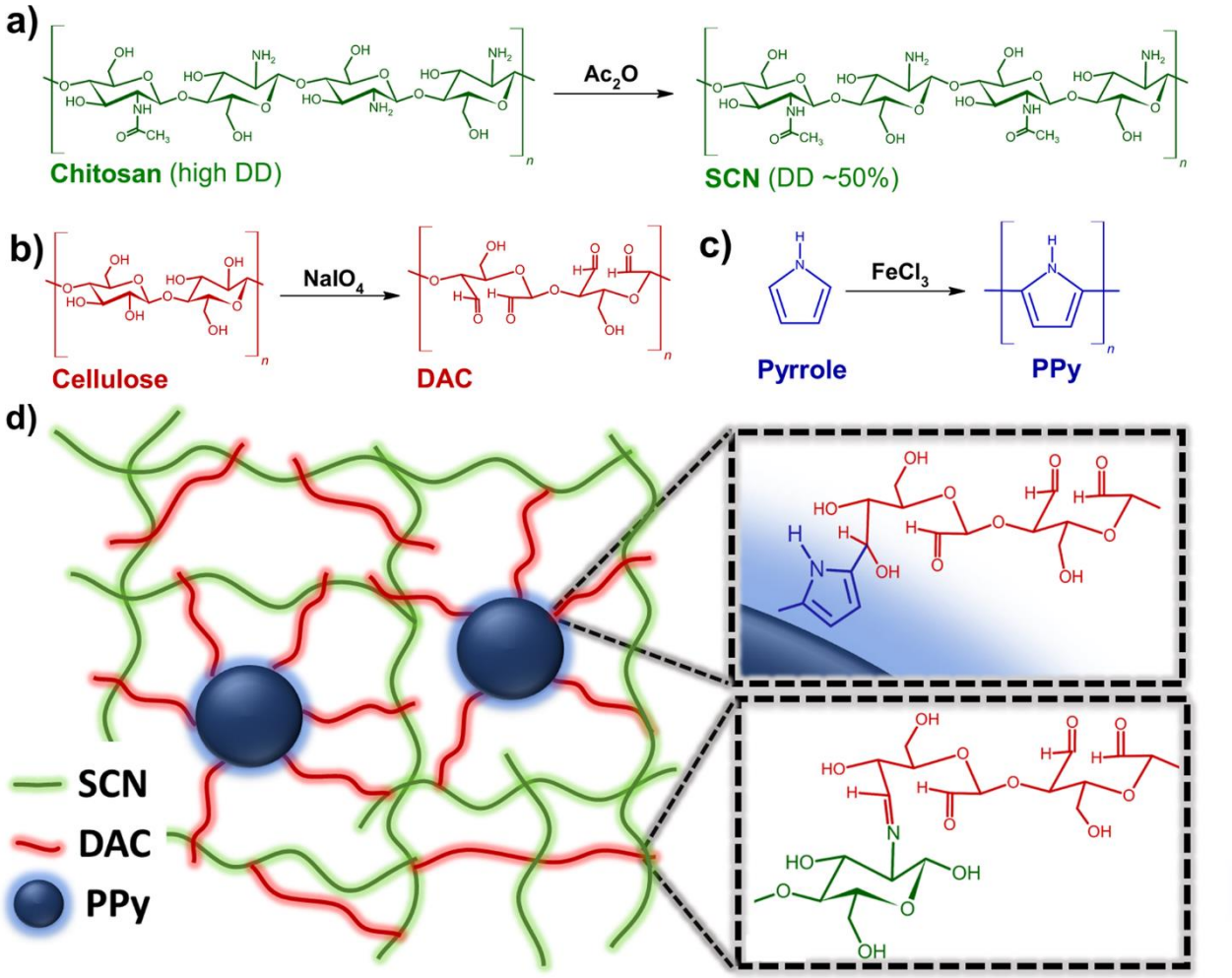

Scheme 1: Scheme of a) Synthesis of SCN, b) synthesis of DAC, c) preparation of PPy. d) representation of SCN/DAC_PPy hydrogel with details of bonding between DAC and PPy (top) and DAC and SCN (bottom).

2. Methods

2.1 Materials

Pyrrole (Sigma-Aldrich Co.), iron (III) chloride (Sigma-Aldrich), poly(vinylpyrrolidone) (PVP; Fluka, K 90, molecular weight M_w = 360,000) were used in the preparation of polypyrrole colloids stabilized by poly(vinylpyrrolidone) (PPy/PVP). Cellulose SigmaCell type 20 (weight-average molecular weight M_w = 76 kDa, degree of polymerization DP = 468, dispersity $Đ$ = 4.7; Sigma Aldrich Co.), sodium periodate ($NaIO_4$; Penta, Czech Republic) and ethylene glycol (Penta, Czech Republic) were used in the preparation of DAC. Low-molecular weight chitosan (molecular weight 50–190 kDa according to supplier; Sigma Aldrich Co.), glacial acetic acid (CH_3COOH; Sigma Aldrich Co.), absolute ethanol (Et-OH; VWR, Czech Republic), acetic anhydride (Ac_2O; Sigma Aldrich Co.), hydrochloric acid (HCl; Penta, Czech Republic) and sodium hydroxide (NaOH; Penta, Czech Republic) were used in the preparation of SCN. Reagents used for the biological experiments included calf serum (CS, mycoplasma-free; Biosera, France), fetal bovine serum (FBS; PAN, Germany), penicillin-streptomycin (Biosera, France), trypsin (Biosera, France), Dulbecco's Modified Eagle's Medium (DMEM; Gibco), phosphate-buffered saline pH 7.2 (PBS, BioSera,

France), 3-(4,5-dimethylthiazol-2-yl)-2,5-diphenyl tetrazolium bromide (MTT, Duchefa Biochemie B. V., Netherlands) reagent and dimethyl sulfoxide (DMSO, Sigma Aldrich Co.), Hoechst 33258 (Thermo Fisher Scientific, USA) ActinGreen™ 488 or Actin Red 555 (Thermo Fisher Scientific, USA), plate count agar (PCA, HiMedia Laboratories, Mumbai, India), soybean casein digest lecithin polysorbate medium solution (SCDLP M011, HiMedia Laboratories, India). All chemicals were of analytical grade and were used without further purification. Ultrapure water (UPW) with a conductivity below 0.1 µS/cm was used throughout the experiments.

2.2 Synthesis of water-soluble SCN

The half N-acetylated (50%) chitosan was prepared using a modified procedure by Qin et al.(Qin et al., 2006) Briefly, 2.2g low-molecular-weight chitosan was dissolved in 70 mL of 10% acetic acid for 6 h. Then, 50 mL of a mixture of ethanol containing 0.519 mL of Ac_2O was added dropwise and stirred for 15 h at 40 °C. In the next step, the reaction solution was increased by 50 mL of UPW, and the pH was set to 8.5 using 5 M NaOH, which initiated the formation of gel particles in the solution. The mixture was subsequently dialyzed for 72 h. Subsequently, the pH was set to 6.5 which led to the dissolution of gel particles, and the mixture was dialyzed against UPW and 0.1 M NaCl solution, followed again by brief (2 h) dialysis against UPW to desalinate the product. The product was centrifuged (10 000 RPM, 10 min), filtered, and lyophilized.

2.3 Synthesis of DAC macromolecular crosslinker

The 1.65 g of $NaIO_4$ was dissolved in 50 mL of UPW and used for oxidation of 1 g of cellulose (molar ratio of anhydroglucose unit: $NaIO_4$ was 1:1.25).(Münster et al., 2017, 2018) The reaction mixture was stirred at 30 °C in the absence of light for 72 h when it was terminated by the addition of excess ethylene glycol. The resulting DAC was purified by repeated centrifugation and mechanical homogenization using WiseTis homogenizer HD-15 (Witeg, Germany). Next, the purified suspension of the DAC product was transferred into a clear solution via the solubilization process (80 °C for 2 h using an oil bath under reflux). (Kim et al., 2004) The final step involved DAC solution purification by centrifugation and filtration to remove insoluble residues, and dialyzation for 48 h using 14 kDa molecular weight cut-off (*MWCO*) dialysis tubing. The solubilized and purified product was flash-frozen at -80 °C and lyophilized.

2.4 Synthesis of polypyrrole colloids

Solution with a concentration of 2 wt.% of PVP was prepared by dissolving the exact amount of PVP in 25 mL of UPW. Additionally, 0.335 g of pyrrole (5 mmol) was also dissolved in 25 mL of UPW and added to the PVP solution. The mixture was sonicated for 30 min to obtain a homogeneous solution, which was subsequently mixed with 50 mL solution of iron(III) chloride (1.352 g; 5 mmol) in UPW. The mixture was kept undisturbed at room temperature for 24 h. The produced polypyrrole colloidal dispersions (PPy) were poured into a dialysis tube (g (Spectra/Por 1, Spectrum Medical Instruments, USA; 7 kDa *MWCO*) and dialyzed against a large volume of 0.2 M hydrochloric acid to remove any unreacted monomer, and oxidant ions. (Káčerová et al., 2023)

2.5 Preparation of thin hydrogels

The SCN/DAC hydrogels containing 2 and 5 mol.% of DAC relative to SCN (SCN/DAC_2% and SCN/DAC _5%) were prepared by dissolving 200 mg of SCN in 15 mL of UPW, to which a given amount of DAC dissolved in 15 mL of UPW was added. The mixture was briefly but vigorously stirred and subsequently poured into a plastic container with a Teflon bottom of 6.3 cm diameter. The container was covered by a vapor-permeable membrane (6500 g/24 h) to slow down the drying process (prevents the formation of dry-out crust and deformation) and dried at 37 °C in the kiln until constant weight. Dry films

were subsequently washed for 48 h in UPW, cut, and stored in UPW until use. PPy-containing hydrogels were prepared by adding 5 or 10 wt.% of PPy (relative to SCN) to the SCN solution, i.e. the amount of colloid containing 10 or 20 mg of PPy was added to the solution containing 200 mg of SCN (total volume 15 ml), and the mixture was stirred for 24 h. The rest of the procedure was identical to the preparation of pure SCN/DAC hydrogels. These hydrogels are in the following noted as SCN/DAC_PPy5% and SCN/DAC_PPy10%.

2.6 Physico-chemical characterization of prepared materials

UV/VIS, FT-IR, and Raman spectral analysis. Double-beam UV/VIS spectrometer Lambda 1050 (PerkinElmer, USA) was utilized in a span of wavelengths 180–800 nm for the analysis of the periodate consumption during the oxidation of cellulose to DAC, employing measurements of aliquot samples collected in a timeframe ranging from 15 min to 96 h after the periodate oxidation initiation. Qualitative FT-IR analysis was performed using the infrared spectrometer Nicolet 6700 FT-IR (Thermo Fisher Scientific, USA) equipped with the diamond crystal in the ATR mode in a span of wavenumbers 4000–700 cm^{-1} (res.: 4, scans: 64). For results of both spectral analyses see Support Information (SI). Raman spectra of DAC, PPy, and PPy+DAC (1:10) in solutions were collected using Nicolet DXR Raman microscope (Thermo Scientific) with excitation laser 455 nm. 1000 spectral scans with exposures of 2 s/scan were set for each spectrum measurement. Obtained data were corrected with a standard correction procedure implemented in the Omnic software (Thermo Fisher Scientific, USA) to minimize the effect of fluorescence.

NMR measurements. The ^{1}H and ^{1}H-^{13}C HSQC correlation spectra were obtained for 10 mg/mL SCN samples using a recorded using a JEOL 400 MHz NMR spectrometer (JEOL, Japan). The measurements were performed at T = 298 K in D2O. The ^{1}H–^{13}C heteronuclear single quantum correlation (HSQC, J_{H-C} = 145 Hz) experiments were used based on previous experiences. (Münster et al., 2017, 2021)

TEM analysis. Transmission electron microscopy (TEM) analysis of the PPy sample was carried out using a JEM-2100 transmission microscope (JEOL, Japan) operated at an acceleration voltage of 160 keV. The samples were drop-cast from diluted aqueous suspension onto a 300 mesh copper grid coated with Formvar membrane and gently dried.

DLS analysis. Zeta potential (ζ) and hydrodynamic radius of the PPy sample were determined by dynamic light scattering (DLS) on a Zetasizer Nano ZS90 instrument (Malvern Instruments, UK) at 25 °C using DTS1070 cells and the Smoluchowski model. The concentration of PPy in the samples was set to 1.87 mg/mL.

Hydrogel network parameters. The network parameters were estimated based on the weight changes during swelling experiments on prepared d = 15 mm disc-shaped SCN/DAC and SCN/DAC_PPy hydrogels. The hydrogel discs were thoroughly washed in UPW with regular changing of UPW. Subsequently, the swollen discs were gently dried to remove excess water, weighed, and lyophilized. The network parameters were determined using the equilibrium swelling theory proposed by Flory and Rehner (1943).(Flory & Rehner, 1943) Following equations were used to calculate network parameters.

Percentage of swelling, where M_E is the mass of the hydrogel swollen to the equilibrium state, and M_0 is the mass of the washed and dried hydrogel.

$$\text{Percentage of swelling (\%)} = \frac{M_E - M_0}{M_0} \times 100 \quad (1)$$

Equilibrium water content (*EWC*) describes the maximum amount of water absorbed by the hydrogel. M_s is the mass of the sample swelled under equilibrium conditions, and M_0 is the mass of the washed and dried hydrogel.

$$EWC\ (\%) = \frac{M_s - M_0}{M_s} \times 100 \quad (2)$$

The gel fraction, where M_0 is the weight of the dried hydrogel after extraction of the soluble fraction in the hydrogel and M_{int} is the weight of the dry and non-washed hydrogel.

$$\text{Gel fraction}\ (\%) = \frac{M_0}{M_{int}} \times 100 \quad (3)$$

Analysis of viscoelastic properties. Disc-shaped SCN/DAC and SCN/DAC_PPy hydrogel samples (d = 15 mm) were measured in an equilibrium swollen state using a rotational rheometer Anton Paar MCR 502 (Anton Paar, Austria) equipped with a D-PP15 shaft using a roughened aluminum plate with 15 mm diameter and ground plate with glued sandpaper both used to prevent slipping of samples during measurement. The measurement was performed in oscillation mode in frequency sweep from 1 to 10 Hz by applying a constant strain of 1%.

SEM analysis. SCN/DAC and SCN/DAC_PPy washed and lyophilized cryogels were analyzed by scanning electron microscope Nova NanoSEM 450 (FEI, Czech Republic) operated at 5 kV accelerating voltage. All specimens intended for SEM analysis were sputtered by gold-palladium nanoparticles to prevent the charge accumulation effect.

2.7 Conductivity

The conductivity of the samples was determined by the two-probe van der Pauw method using a digital electrometer Keithly 6517B. The measurements were accomplished at room temperature.

2.8 Evaluation of cytocompatibility

The cytocompatibility of scaffolds was evaluated by the determination of cytotoxicity and proliferation activity. While the first is related to safety evaluation, the second shows the ability of cells to grow in direct contact with the material.

Cytotoxicity: The cytotoxicity evaluation was performed following ISO 10993 standards using a mouse embryonic fibroblast cell line NIH/3T3 (ECACC 93061524, England). DMEM with the added content of 10% of the bovine calf serum and penicillin/streptomycin with a final concentration of 100 U/mL was used for the cultivation of NIH/3T3 cells. First, cells were pre-cultivated in the concentration of 1×10^5 cells per mL of media at 37 °C under the 5% CO_2 atmosphere in the humidified air using the HERAcell 150i incubator (Thermo Scientific, USA) for 24 h. Subsequently, the culture medium was replaced with the fresh one, and the tested samples SCN/DAC_2%, SCN/DAC_PPy5%, and SCN/DAC_PPy10% were transferred to the direct contact with pre-cultivated cells. Cells cultivated in a pure medium without the samples were used as a reference. Then, after one day of cell cultivation in the presence of hydrogels, the effect of the samples on the viability and growth of cells was assessed. The assessment of cytotoxic effects was accomplished by using the MTT assay. All assays were performed in quadruplets. Absorption was measured at 570 nm using the Infinite M200 Pro NanoQuant (Tecan, Switzerland). The cytotoxic effect was evaluated according to the ISO 10993, part 5. Viability higher than 0.7 was assumed as the absence of cytotoxicity, and viability lower than 0.7 was evaluated as cytotoxic.

Cell proliferation in direct contact with material: The mouse embryonic fibroblast cell line NIH/3T3 (ECACC 93061524, England) was also used for the proliferation tests. The cells were seeded on the samples in the concentration of 1×10^5 cells per mL of media and incubated at 37 °C in 5% CO_2 in humidified air. After 72 h of proliferation, the cells were fixed and stained with Hoechst 33258 (blue color) was used for cell nuclei visualization and ActinGreen™ 488 or Actin Red 555 visualized actin filaments. As a reference cells cultured in a pure medium attached to the tissue plate were used. The morphology of the cells was observed using an Olympus Fluoview FV3000 confocal microscope (Olympus, Japan).

2.9 Skin irritation test

An *in vitro* skin irritation test was accomplished. The samples were applied onto a 3D reconstructed human epidermal (RhE) tissue model EpiDerm™ (EPI-200, MatTek, Ashland, USA and MatTek In Vitro Science Laboratories, Bratislava, Slovakia). After 1h of the exposure to the tested substances, RhE was washed with PBS and incubated in a fresh medium for 42 h. In the next step, skin irritation was evaluated using MTT assay. The test was performed according to Epiderm skin irritation test (OECD TG 439). Viability higher than 50% was assumed as the absence of irritation.

2.10 In vitro wound healing promotion

For the evaluation of the wound healing activity, the migration assay was performed.(C.-C. Liang et al., 2007) Concretely, the mouse embryonic fibroblast cell line NIH/3T3 was seeded on the tissue culture dishes at the density of 2×10^5 per mL of media and incubated at 37 °C in 5% CO_2 in humidified air until they reached a confluent monolayer. Subsequently, the monolayer was scratched using a sterile 200 μL pipette tip. The cellular debris was washed away with PBS, and pictures of scratches were taken. Furthermore, fresh medium was added as well as the tested samples. Petri dishes with the cells and samples were incubated at 37 °C in 5% CO_2 in humidified air. The images of the cells were taken at the same position after 10 and 24 h using the phase-contrast Olympus IX81 microscope (Olympus, Japan). The software T-Scratch (CSElab, Switzerland) was used for the analysis and the results are presented as a percentage of open wound areas remaining after 10 and 24 h.

2.11 Antioxidant activity in a luminol-HRP-H_2O_2 cell-free system.

The principle of the method was described previously(Vasicek et al., 2014). As a source of chemiluminescence (CL) signal, the H_2O_2 and horseradish peroxidase (HRP) was used. SCN/DAC_2%, SCN/DAC_PPy5%, or SCN/DAC_PPy10% hydrogels, HRP (final concentration 2 U/mL), and luminol (final concentration 10 μM) were mixed in a 96-well luminescence plate final volume was 200 μL. The reaction was started by adding H_2O_2 to a final concentration of 100 μmol/L. CL signal was measured for 120 min at 37 °C by an LM-01 microplate luminometer (Immunotech, CzechRepublic). Data were converted to a percentage of the control and presented as mean (n = 4) ± SEM.

2.12 Immunomodulatory activity.

The ROS production of isolated neutrophils. Blood samples were collected from the cubital vein of healthy individuals. The volunteers were aged 18–50, both female and male, and they did not take any drugs and were free of any signs of cold or other diseases for at least 3 weeks before blood sampling. Immune cells of healthy donors will be isolated from buffy coats obtained from the Department of Transfusion & Tissue Medicine of the Brno University Hospital, based on an ongoing contract approved by the ethical committee FH Brno. Sodium citrate (0.38% final concentration) was used as an anticoagulant. The whole blood was mixed with 3% dextran and left at room temperature for approx. 30 min. The resulting buffy coat was overlaid on Histopaque 1.077 and centrifuged at 390 g for 30 min without acceleration and brake. After

centrifugation, the remaining erythrocytes were lysed by water hypotonic lysis for 30 sec. The neutrophils were washed in cold PBS, centrifuged at 190 g for 10 min, and finally resuspended in cold PBS. The viability of neutrophils was verified by a CASY cytometer (Roche, Switzerland) and only neutrophils with viability over 95% were used for experiments. Kinetics of ROS formation by isolated neutrophils was determined by luminol-enhanced CL for 120 min at 37 °C, using 96-well white flat-bottom culture plates on a luminometer (Immunotech, the Czech Republic and Infinite M200, Tecan, Switzerland). The analysis was performed according to Georgiev et al.(Georgiev et al., 2017) Firstly, 25 μL of neutrophil suspension (2.5×10^5 cells/well) in Hank's buffered salt solution (HBSS) was mixed with 25 μL of 10 mM luminol (in 0.2 M borate buffer), and the hydrogels containing 0 (SCN/DAC_2%), 5% (SCN/DAC_PPy5%) and 10% of PPy (SCN/DAC_Ppy10%), respectively. The total reaction volume was adjusted to 250 μL with HBSS and the samples were measured immediately. The response obtained was named spontaneous (non-stimulated with other activators) CL. Secondly, 25 μL of neutrophil suspension (2.5×10^5 cells/well) mixed with 25 μL of 10 mM luminol and SCN/DAC_2%, SCN/DAC_PPy5%, or SCN/DAC_PPy10%, were activated with 25 μL of 62.5 μg/mL opsonized zymosan particles (OZP-activated CL, Sigma-Aldrich). HBSS was also used to adjust the total reaction volume to 250 μL. The data were based on integral values of CL over 120 min. and converted to a percentage of the respective control (without or with OZP) and presented as mean (n = 4) ± standard error of the mean (SEM).

Viability of RAW cells. Cell viability of murine peritoneal macrophage RAW264.7 (European Collection of Authenticated Cell Culture, UK) cells was based on the determination of the amount of metabolically active cells according to the analysis of the total amount of MTT or related tetrazolium salts in whole-cell lysates, which reflects the number of metabolically active viable cells in culture, as described in Moosova et al.(Moosova et al., 2019) Cells were cultured in DMEM supplemented with 10% of heat-inactivated low endotoxin FBS and 1% combination penicillin-streptomycin. To determine the effect of the tested hydrogels, macrophages were incubated with the hydrogels alone and in combination with the lipopolysaccharide (LPS) macrophage activator. For the first setup without an LPS activator, murine macrophage cell line RAW 264.7 was cultured in 24-well flat-bottom plates at 2.5×10^5 cells/well, covered by the SCN/DAC_2%, SCN/DAC_PPy5%, or SCN/DAC_PPy10% hydrogels and incubated for 24 h. The total volume in each well was 500 μL. For the second setup with LPS activation, 15 ng/mL LPS (*E. coli*/026:B6, Sigma-Aldrich Co.) was added to the macrophages and the tested hydrogels and incubated for 24 h at 37°C in an atmosphere of 5% CO_2 and 95% air. At the end of the incubation period, MTT assay was performed. The resulting absorbance was read at 570 nm on a SPECTRA Sunrise microplate reader (Tecan, Mannedorf, Switzerland). Data were converted of the respective control (without or with LPS) and presented as mean (n=4) ± SEM.

2.13 Nitric oxide (NO) and interleukin 6 (IL-6) production from murine macrophages.

Changes in NO production were measured indirectly as the accumulation of nitrites (the end product of NO metabolism) in the medium by using Griess reagent (Sigma-Aldrich Co.), according to the method described previously.(Vasicek et al., 2020) To determine the effect of the tested hydrogels, macrophages were incubated with the hydrogels alone and in combination with the lipopolysaccharide (LPS) macrophage activator. For the first setup without an LPS activator, murine macrophage cell line RAW 264.7 was cultured in 24-well flat-bottom plates at 2.5×10^5 cells/well, covered by the tested hydrogels and incubated for 24 h. The total volume in each well was 500 μL. For the second setup with LPS activation, 15 ng/mL LPS (*E. coli*/026:B6, Sigma-Aldrich Co.) was added to the macrophages and the tested hydrogels and incubated for 24 h. At the end of both incubations, the supernatants were collected by centrifugation at 16,000 g at 4 °C for 5 minutes and 80 μL of each sample was mixed with an equal volume of the Griess reagent in a 96-well plate. The reaction mixtures were incubated at room temperature for 30 min in the dark and the absorbance was read at 540 nm. A standard curve of 0–52 μM $NaNO_2$ was prepared and used for calculations. Data were converted of the respective control (without or with LPS) and presented as mean (n = 4) ± SEM.

The concentration of pro-inflammatory cytokine IL-6 produced by RAW264.7 cells into the cultivation medium was determined after 24 h of exposure to tested hydrogels and LPS by commercially available immunoassays (Mouse IL-6 DuoSet, R&D Systems). The assays were performed according to the manufacturer's instructions as described previously.(Vasicek et al., 2020) Data were converted of the respective control (without or with LPS) and presented as mean (n = 4) ± SEM.

2.14 Antibacterial activity

Antibacterial activity was assessed using gram-positive bacteria *Staphylococcus aureus* CCM 4516 and gram-negative bacteria *Escherichia coli* CCM 4517 obtained from the Czech Collection of Microorganisms (CCM, Brno, Czech Republic), and grown on the plate count agar PCA. Antibacterial activity was tested according to ISO 22196 with modifications. Sterile hydrogels with dimensions of 25 × 25 mm^2 were inoculated with 0.1 mL of a required bacterial suspension, specifically *Streptococcus aureus* (5.0×10^5 cfu/mL) and *Escherichia coli* (4.6×10^5 cfu/mL). Next, the inoculated samples were covered with polypropylene film (20 × 20 mm^2). The samples were incubated at 35 °C for 24 h and relative humidity of 95%. In the next step, polypropylene films were removed and the samples were rinsed with 2.5 mL of SCDLP and a dilution series from 0 to 10^{-7} was prepared from the prepared microbial suspension and phosphate buffered physiological saline. One mL of each dilution was mixed together with the samples in the separate Petri dishes. All the plates were incubated at 35 °C for 24-48 h. After the incubation, bacterial colonies were counted and recorded. The value of antimicrobial activity was calculated according to the formula of Equation (4).

$$R = U_t - A_t \tag{4}$$

Where R is antimicrobial activity; U_t is the average value of the logarithm of viable bacteria in units of cells/cm^2 of untreated test samples after 24 h of incubation; and A_t is the average value of the logarithm of viable bacteria units of cells/cm^2 of test specimens after 24 h of incubation. All the tests were run in duplicates and neat hydrogel SCN/DAC was used as a reference.

2.15 Statistical analysis.

Data are presented as mean ± SEM. All assays were performed in quadruplicates. The number of independent experiments (n) is stated in the figure legend. The data from some of the measurements were normalized to the reference in each experiment to account for the variability of individual cell passages. Statistical analysis was performed using GraphPad Prism version 6.01 for Windows. Statistical differences were tested by one-way ANOVA, which was followed by Dunnett's multiple comparison test or by a one-sample t-test to compare values expressed as percentages. In the case of one sample t-test application, the Bonferroni correction of the p-value for multiple comparisons was performed. $P < 0.05$ was taken to indicate significant differences between data mean values.

3. Results and discussion

3.1 Characterization of SCN, DAC, and PPy

Water soluble half N-acetylated chitosan (SCN) was prepared according to the modified procedure of Qin et al., (Qin et al., 2006) while the DAC and PPy colloids were prepared following our earlier works. (Káčerová et al., 2023; Muchová et al., 2022; Münster et al., 2017) FT-IR spectrum of source chitosan, SCN, source cellulose, and DAC are given in Figure S1 in SI. Partial (re)acetylation of chitosan resulted in increased intensity of amide-group vibration bands, particularly the Amide I (1640 cm^{-1}) and Amide II (1530

cm^{-1}), which agrees with an increased amount of N-acetylglucosamine groups. The oxidation of cellulose to DAC is confirmed by the appearance of bands around 1730 cm^{-1} (C=O) and 877 cm^{-1} (hemiacetal C–O–C) vibrations.

The ^{1}H NMR spectrum of SCN is in Figure 1a and the ^{1}H-^{13}C HSQC spectrum is given in Figure S2. The signal assignment is based on Kubota et al. (Kubota et al., 2000) and the degree of deacetylation (DD = 57%) was established according to Kasaai (Kasaai, 2010) as a comparison of 1/3 of the signal intensity of $CH_{3(N\text{-}ac)}$ and the 1/6 of the sum of H2–H6 intensities. Despite somewhat higher residual DD, the SCN is highly soluble in water at neutral pH and in PBS of pH 7.4.

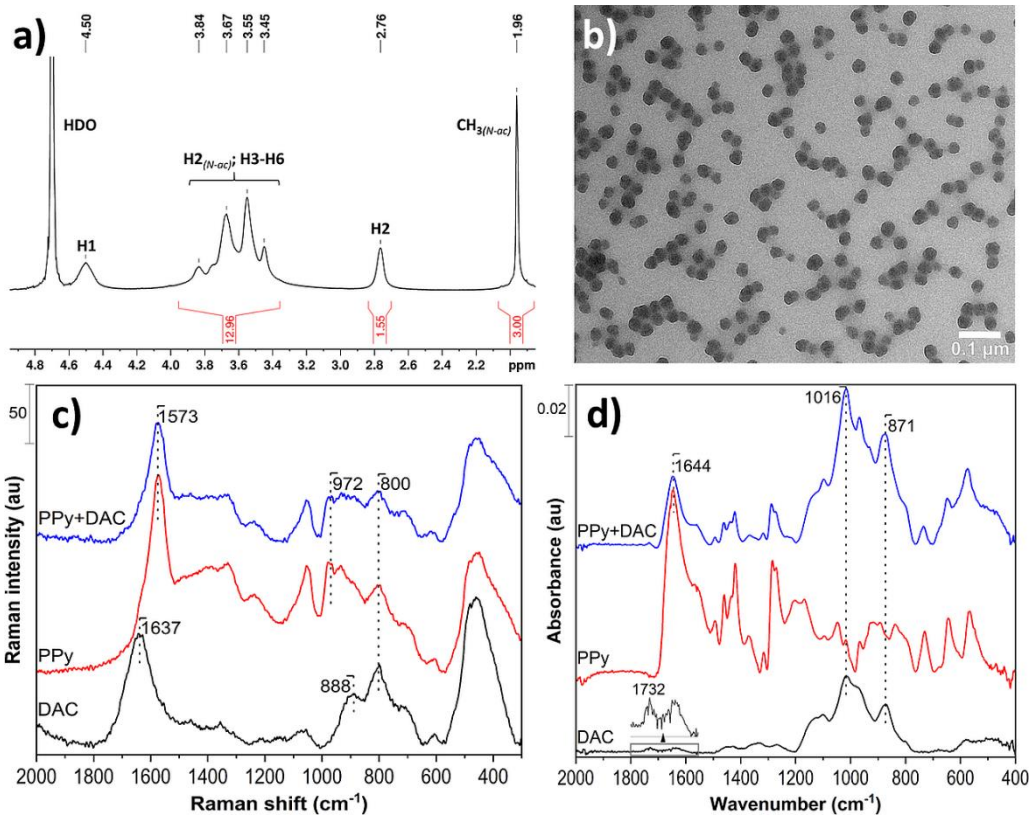

Figure 1: a) ^{1}H NMR spectrum of SCN, b) TEM of PPy colloid, c) Raman spectra of DAC, PPy, and their 10 : 1 mixture in UPW (PPy+DAC), d) FT-IR spectra of DAC, PPy and dried-out PPy+DAC mixture.

Polypyrrole colloid stabilized by poly(vinyl pyrrolidone), hitherto known as PPy, was synthesized and characterized by TEM analysis which revealed the presence of spherical 37 ± 4 nm large particles, Figure 1b. The hydrodynamic diameter of the particles in UPW was 170±3 nm according to DLS, with $Đ$ = 0.269. Colloid had a final concentration of 21.9 mg particles/mL and was stable for several months when stored at 4 °C (179±2 nm) as well as under biological conditions (PBS, pH 7.4, 37°C).

3.2. PPy – DAC reaction

While the Schiff base formation between aldehydes and $–NH_2$ groups is widely used for hydrogel crosslinking, the covalent anchoring of PPy by DAC has not been described before and is thus investigated more closely. The proof of spontaneous DAC-PPy reaction was obtained from a comparison of Raman and IR spectra of DAC, PPy, and their aqueous mixtures which reacted for 24 h (Raman) and were subsequently dried out (FT-IR), see Figure 1c,d. The 10:1 DAC: PPy w/w ratio has been chosen to maximize the intensity

of DAC vibrations in the DAC+PPy spectra. Even at such a high reactant ratio, the mixing of DAC and PPy resulted in the disappearance of the band of free DAC carbonyl groups, located at 1637 cm^{-1} in Raman and 1732 cm^{-1} in FT-IR spectra of DAC. This is particularly well visible in Raman spectra due to the rather low intensity of DAC carbonyl vibration in FT-IR spectra. Also, note that other bands of DAC located between 800 and 1200 cm^{-1} are still clearly visible in both Raman and FT-IR DAC+PPy spectra. The selective disappearance of bands related to aldehyde groups are a clear indication of the reaction between –CHO of DAC and the PPy.

Given the tendency of pyrrole to react with electrophiles at the α position due to the highest stability of intermediates, the reaction between the –CHO group of DAC and free α carbons at the end of PPy chains is presumed. According to the literature, a condensation reaction between aldehydes and the Cα of pyrrole is used in organic chemistry for the preparation of pyrrole oligomers and derivatives.(Iii & S. Lindsey, 2001) It runs spontaneously at normal temperature in water with quantitative yield.(Gu et al., 2015) Moreover, aldehyde-pyrrole condensation is used to insert various aromatic groups into the PPy chains during their polymerization, thus modifying their properties.(W. Zhao et al., 2017) It is therefore assumed that a similar condensation reaction takes place also in the case of DAC and PPy. A more extensive study of this reaction is currently underway.

3.3. Characterization of SCN/DAC hydrogels

Initially, the SCN/DAC hydrogels with different amounts of DAC (2 and 5 mol.%) were investigated to determine the optimal amount of crosslinker. The study of network parameters revealed successful hydrogel formation in both cases. The SCN/DAC_2% sample swelled 31±6 times its dry weight and has an equilibrium water content (EWC) of 96±2%. The more crosslinked sample with 5% DAC swelled significantly less (7.5±0.7 times its dry weight) and had an EWC of 88±1%. The gel fraction of the hydrogel samples was 80 ± 1% and 84±3%, for 2 and 5% of DAC, respectively. The rheological investigation, namely the dominance of G' over G'' reflected also in $tan\theta < 1$, further confirmed the formation of a crosslinked hydrogel network (Figure S3 in SI). The values of storage modulus G', loss modulus G'', complex modulus G*, and damping factor $tan\theta$ scaled with increasing DAC concentration. The 2% DAC hydrogel sample was found to be significantly less elastic than the 5% one. Both hydrogels were also easy to handle without tearing, despite their relatively low thickness (~1 mm in the swelled state).

The cytotoxicity of SCN/DAC hydrogels in direct contact with the mouse embryonic fibroblast cell line NIH/3T3 was evaluated according to ISO 10993-5 (Figure S4). Neither sample showed significant cytotoxicity toward the selected cell line. The growth of the cells on the hydrogel surface and in their presence was studied by confocal microscopy (Figure S4). While only isolated cell clusters were found on the surface of the 2% SCN/DAC hydrogel, the 5% SCN/DAC hydrogel supported cellular growth better. The growth in the presence of both hydrogels was unimpeded in both cases and fibroblasts retained their physiological morphology.

Despite the good results of both hydrogels, only the SCN/DAC_2% hydrogel was selected for incorporation of PPy colloids based on: i) its lower elasticity compared to SCN/DAC_5% allowing better adhesion to the uneven surface of the skin or wound, ii) higher swelling capacity for better exudate absorption, iii) lower cell attachment and growth on its surface, which prevents the dressing being ingrown into the wound.

3.4 Characterization of SCN/DAC hydrogels with PPy

The PPy-containing composite hydrogels based on SCN/DAC_2% are in the following referred to as SCN/DAC_PPy5% (containing 5 wt.% of PPy relative to SCN) and SCN/DAC_PPy10% (containing 10

wt.% of PPy relative to SCN). Evaluation of network parameters revealed that SCN/DAC_PPy5% swelled approximately the same as SCN/DAC_2% (31±9 times), had EWC of 97±1%, and gel fraction of 59±2 %, while SCN/DAC_PPy10% swelled significantly more (77±9 times), had highest EWC of 99±0.2% and gel fraction of 62±2%. The storage modulus G', loss modulus G'', complex modulus G*, and damping factor *tanθ* of PPy hydrogels are given in Figure 2 and compared with SCN/DAC_2%. The photographs of prepared hydrogel samples are given in Figure 3a.

The storage, loss, and complex moduli of both PPy-containing hydrogels are higher than in the case of SCN/DAC_2% despite the same amount of crosslinker. This could be explained by the incorporation of stiffer PPy particles into the network. Note, however, that rheological parameters do not scale with the increasing amount of PPy as one may expect in such a case. The sample containing 10 wt.% of PPy has, for instance, a significantly lower storage modulus than the SCN/DAC_PPy5%, which indicates decreased crosslinking density in the hydrogel as a sparser network could store less deformation energy. These findings correspond with increased swelling of SCN/DAC_PPy10% and could be justified by an increased PPy: DAC ratio - the greater availability of pyrrole groups for aldehyde condensation means that a higher portion of DAC could bind on the PPy particles and is thus less available for crosslinking of SCN chains. The preference for DAC-PPy reaction over the Schiff base formation is likely given by the dynamic nature of the latter. As Schiff bonds constantly break and reform during the hydrogel's drying, part of the freed aldehyde groups of DAC may interact with nearby PPy and form classic permanent covalent linkages, thus shifting the equilibrium between the reactions towards the condensation. In case of an abundance of PPy particles, most of the DAC would thus be bonded to their surface embedded in SCN. Such a locally dense network would explain observed rheological and swelling behavior as well as the rather easy tearing of SCN/DAC_PPy10% samples during manipulation. SCN/DAC_PPy10% sample was much less resilient than the SCN/DAC_2% sample, which has about two times lower storage modulus. These results provide another proof of the reaction between DAC and PPy.

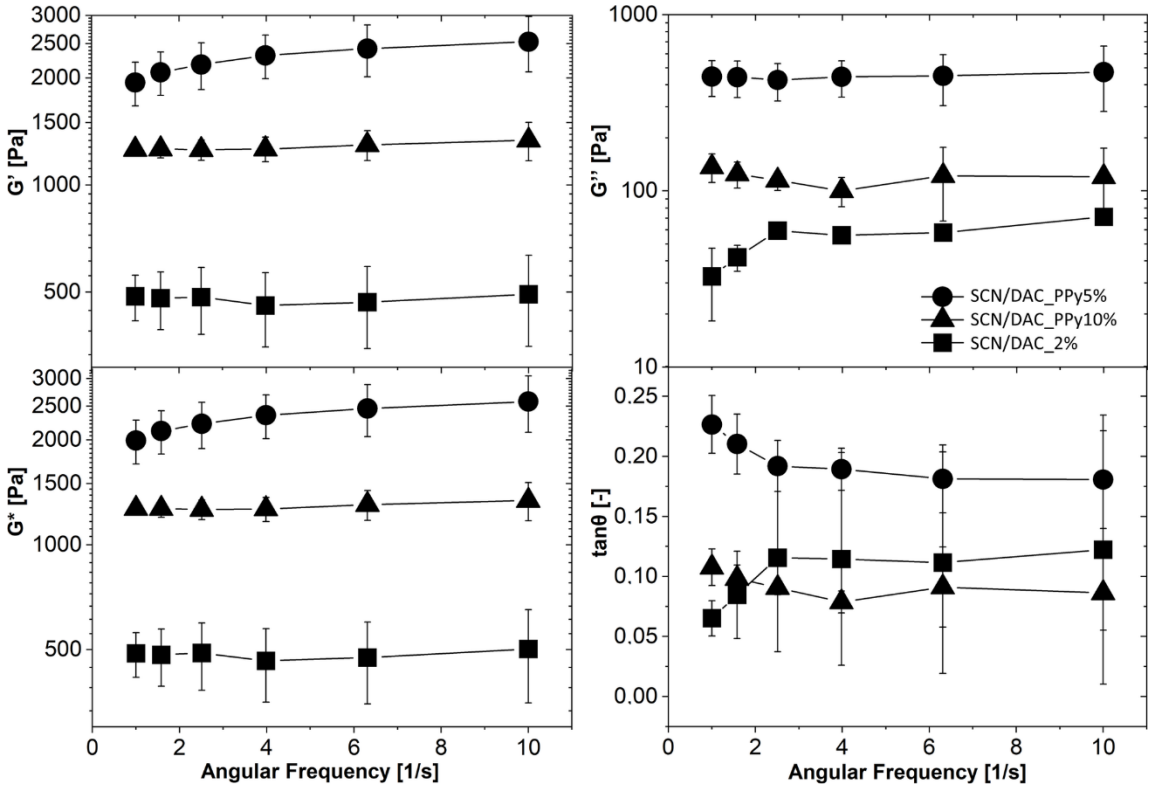

Figure 2: Storage, loss, and complex moduli and damping factor of SCN/DAC_2% and PPy-containing hydrogels prepared using 5 and 10 wt.% of PPy (SCN/DAC_PPy5% and SCN/DAC_PPy10%).

The specific conductivity (K) of the samples was evaluated next (Figure 3b). Due to the combined ionic/electronic conductivity mechanism of PPy colloids, no specific conductivity was observed for dry films, i.e. in the absence of an ion-conducting environment. On the other hand, K of hydrogels swelled in UPW scaled from 2.0 mS/cm for SCN/DAC_2% to 5.1 mS/cm for SCN/DAC_PPy10%, i.e with an increasing amount of PPy. The conductivity of the hydrogels is thus comparable to the conductivity of human tissues, e.g. human muscle (4.1 mS/cm), human dermis (2.2 mS/cm), and epidermis (0.26 mS/cm). (Duck, 1990; Peters et al., 2001) Hydrogels with such a level of conductivity should be capable of transferring the bioelectrical signals and promoting the wound healing process. (X. Zhao et al., 2017) Hydrogels also showed good adherence to the human skin and were able to follow its movements without breaking, as is shown for SCN/DAC_PPy5% in Figure 3c.

The SEM micrographs of the dried films show various amounts of conductive PPy particles (bright dots in Figure 3d and e; the amount depends on the initial dose of PPy colloid) well dispersed in the samples. No aggregation or clustering of particles has been observed; the dispersion of PPy particles in the hydrogel matrix is rather homogeneous. These findings demonstrate the advantages of the adopted methodology, in which given amounts of pre-made PPy colloids of desired qualities are blended into the hydrogel matrix and covalently anchored only after the addition of DAC, i.e. during the hydrogel crosslinking.

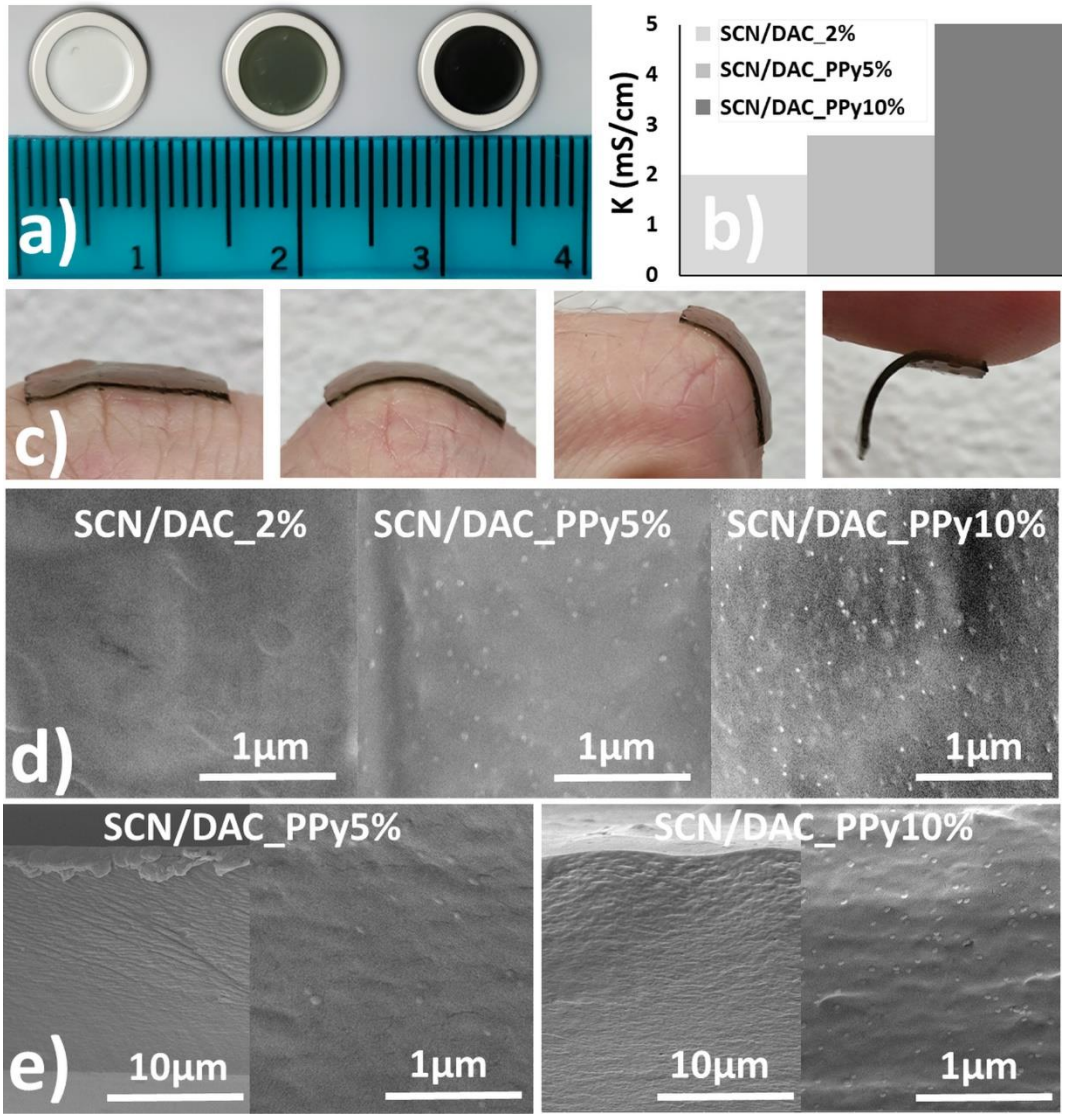

Figure 3: a) photographs of SCN/DAC_2%, SCN/DAC_PPy5%, and SCN/DAC_PPy10% (left to right); b) specific conductivity of the samples (mS/cm^{-1}), c) examples of SCN/DAC_PPy5% adhesion to the skin; SEM images of the d) surface and e) cross sections of dried samples showing the uniform distribution of PPy particles (bright spots) in the hydrogel network.

3.5 Biological evaluation

As discussed in the introduction, wound healing consists of four overlapping phases – homeostasis, inflammation, proliferation, and remodeling. (Guo & DiPietro, 2010) After homeostasis, signaling molecules (e.g. cytokines) are released to control the inflammatory response and activate phagocytosis. IL-6 plays an important role in inflammation as it modulates immune responses. In this stage, macrophages also have a key role as they promote the anti-inflammation effect, and phagocytize bacteria and cell debris. Nitric oxide (NO) plays a key role in the regulation of three major parts of the wound-healing process: vascular homeostasis, inflammation, and antimicrobial action. NO impacts vascular homeostasis, which is disrupted in the event of an injury. Upon tissue injury, a healthy healing process depends upon platelet aggregation and blood clot formation to stop further blood loss. NO also prevents platelet adhesion to the

vessel walls. (Malone-Povolny et al., 2019) A few days after the wounding, fibroblasts begin the re-epithelization phase, and the healing is subsequently completed by the remodeling of new tissue. The selected *in vitro* biological tests reflect individual stages of wound healing to show the potential of prepared hydrogels for possible future preparation of wound dressings. The tests start with a fundamental assessment of cytotoxicity and fibroblast proliferation in the presence of hydrogel. This is followed by the evaluation of the ability of cells to migrate and close a wound using a scratch assay as an *in vitro* model. (C.-C. Liang et al., 2007) Furthermore, the skin irritation test is assessed using the reconstructed human tissue model EpiDerm™. Next, ROS scavaging ability and the impact of hydrogels on neutrophil and macrophage activity are evaluated, as well as the assessment of the hydrogel's antibacterial activity.

Cytocompatibility: absence of cytotoxicity and limited cell ingrowth

The evaluation of cytotoxicity in the presence of SCN/DAC_PPy5% and SCN/DAC_PPy10% was performed according to ISO 10993-5 using an NIH/3T3 cell line.

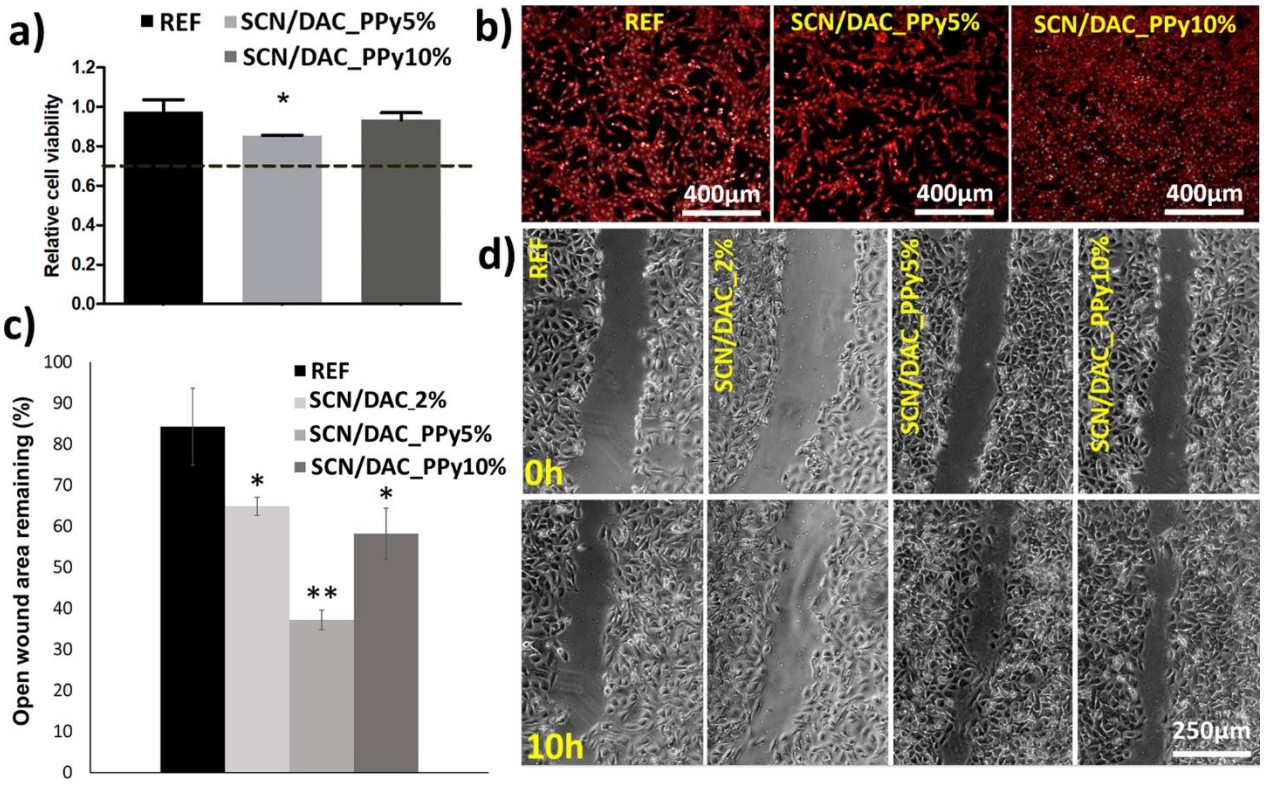

Figure 4: Biological evaluation of SCN/DAC_2%, SCN/DAC_PPy5%, and SCN/DAC_PPy10% using NIH/3T3 cell line; a) the cytotoxicity of SCN/DAC_PPy5%, and SCN/DAC_PPy10% in direct contact; dashed line represents the cytotoxicity threshold according to ISO 10993-5; for comparison with SCN/DAC_2% and SCN_DAC_5% hydrogels see Figure S4a in SI, b) cell growth on the culture plastic in the contact with the samples; for comparison with SCN/DAC_2% and SCN_DAC_5% see Figure S4c in SI, c) open area of the wound remaining [%] after the incubation in the presence of SCN/DAC_2%, SCN/DAC_PPy5%, and SCN/DAC_PPy10% samples for 10h (lower is better), d) representative figures of the wound after 0 h (top) and 10h (bottom row). To determine statistical differences between samples ANOVA with post hoc Tukey's Multiple Comparison test (* $p < 0.05$; ** $p < 0.01$) was performed.

Neither sample showed significant cytotoxicity (Figure 4a) and determined cell viabilities are comparable with neat SCN/DAC hydrogels (Figure S4 in SI). It means that the presence of PPy does not change the cytotoxicity of the neat hydrogel. This is in agreement with previously described PPy properties. (Káčerová et al., 2023) While the absence of cytotoxicity is a main requirement for any biomedical application, the ability of cells to adhere and proliferate on the surface of the material shows the more intimate impact of the material on cell behavior. It can be concluded, that the morphology of fibroblasts on the surface of PPy-containing hydrogels was also physiological (Figure 4b). The adhesion of cells to the surface of the hydrogels was limited, particularly for SCN/DAC_PPy5%, which however can be beneficial for possible future application as removable wound healing patches because their ingrowth is limited. The cytotoxicity results of PPy-containing samples are thus similar to those of neat SCN/DAC hydrogels and the addition of PPy particles had no additional cytotoxic or anti-proliferative effect on the employed cell line.

Skin irritation test: samples show non-irritation characteristics

Induction of skin irritation of topically applied material is a crucial consideration in the safety evaluation. Thus, the skin irritation test conducted on the 3D reconstructed human epidermal (RhE) tissue model EpiDerm™ was studied. Neat SCN/DAC hydrogel and the SCN/DAC_PPy5% sample were selected for testing as reference material and the most promising composite, respectively. Both materials were evaluated as non-irritating, as the cell viability in the RhE of SCN/DAC was 101 ± 4 % and SCN/DAC_PPy5% reached 97 ± 4% (Figure 5).

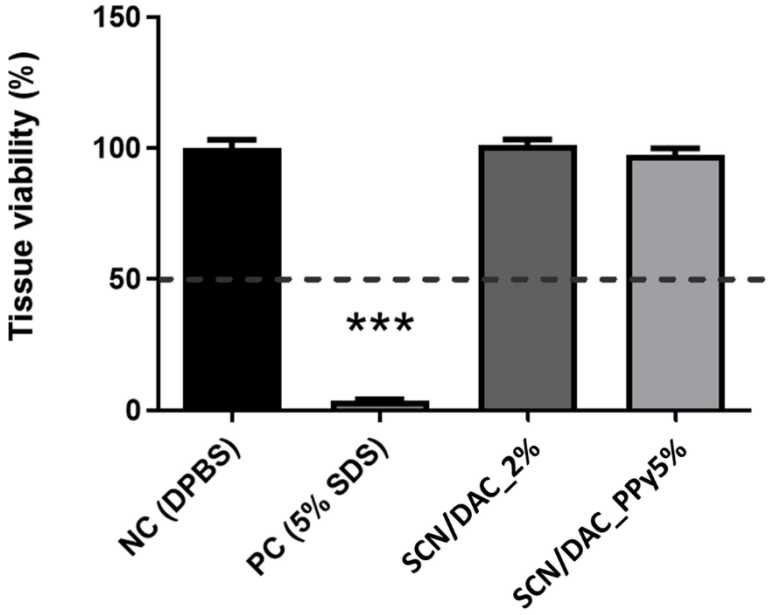

Figure 5: Skin irritation (tissue viability) of SCN/DAC_2% and SCN/DAC_PPy5% hydrogels containing 0% and 5% of PPy. The dashed line highlights the limit of viability according to Globally Harmonised System (GHS, R38, Category 2 or Irritant I), viability < 50% corresponds to irritation. Data were converted to a percentage of the negative control NC (DPBS) and expressed as the mean ± SEM (n = 3). One sample t-test was used to analyze the significance of the obtained data separately comparing the effect of each compound with the NC. To determine statistical differences between samples, an ANOVA test with post hoc Tukey's Multiple Comparison (*** $p < 0.001$) was performed.

The scratch assay proves the improvement of wound healing properties in vitro

Next, the effect of neat SCN/DAC_2% and both PPy-containing hydrogels on wound healing *in vitro* was evaluated using a well-established scratch assay based on the evaluation of NIH/3T3 cells migration, (C.-C. Liang et al., 2007) see Figure 4c,d. The percentage of open wound area remaining after 10 h of incubation was 84±9% for reference, 65±2% for SCN/DAC_2%, 58±6% for SCN/DAC_PPy10%, and only 37±2% for SCN/DAC_PPy5%. Besides, the scratch in the presence of hydrogels also became fully closed within 24 h, while 15% of the open area was still open in the reference. The presence of all tested hydrogel samples thus significantly accelerated the wound healing *in vitro* and enhanced the wound closure rates. Interestingly, the highest wound healing acceleration, i.e. the lowest percentage of open wound area remaining, was found for SCN/DAC_PPy5%, while the wound healing provided by the PPy10% sample was comparable to neat SCN/DAC hydrogel. Although the reason for this behavior is unclear, it seems that the wound healing rate does not scale with the amount of PPy as no benefit of a higher PPy amount was observed. On the other hand, PPy in lower amounts (5 wt.%) significantly enhanced the wound-healing effect of SCN *in vitro*, thus showing an interesting synergy.

Hydrogels show good antioxidant activity

The antioxidant activity plays an important role in the control of immune response – a key phase of the wound healing process. Therefore, we focused on the detection of the antioxidant activity of the tested hydrogels using a luminol-horseradish peroxidase-H_2O_2 cell-free system. Generally, the antioxidative activity of the given compound is related to its ability to donate electrons or reduce/capture free radicals. The antioxidative activity of chitosan is linked to its amine groups. Chitosans with high DD and low M_w thus show the highest antioxidative activity. (Muthu et al., 2021) Although the antioxidative activity of SCN hydrogels has not been tested before, the SCN itself is also known to possess significant antioxidative activity towards various radicals (T. Feng et al., 2006). PPy is a redox-active electron-rich polymer, which could serve both as a donor of electrons and H^+. (Nazarzadeh Zare et al., 2014) It is thus a very potent ROS scavenger, particularly in biological systems, where it showed higher antioxidative activity than polyaniline. (Gizdavic-Nikolaidis et al., 2004)

Both neat and PPy-containing hydrogels showed significant antioxidant activity (Figure 6). The SCN/DAC hydrogels without bound PPy reduced the signal to 63% of control, which confirms earlier findings regarding the antioxidative capabilities of SCN. (T. Feng et al., 2006) The 5% and 10% PPy-containing hydrogels, however, reduced the signal nearly twice as more, to 32% and 30% of the control, respectively. Note, that an increased amount of PPy did not lead to a further increase in antioxidant activity; the results of both PPy-containing hydrogels were comparable. Once again, the synergic effect of PPy particles and SCN has been observed.

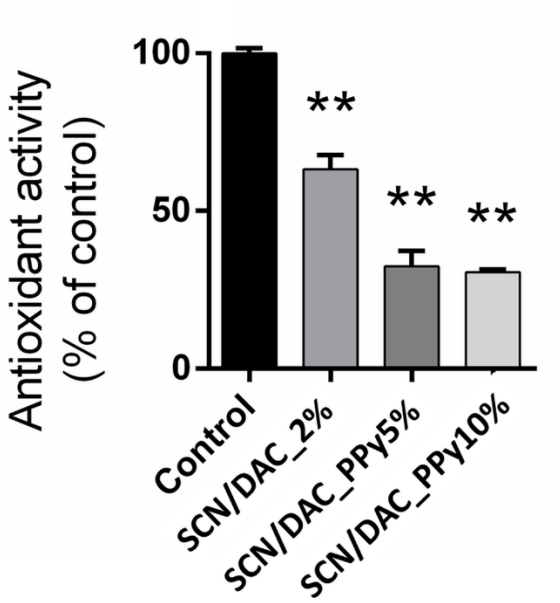

Figure 6: The antioxidant activity of SCN/DAC_2%, SCN/DAC_PPy5%, and SCN/DAC_PPy10% hydrogels with 0, 5, and 10% of PPy. Data were converted to a percentage of the control (without hydrogels) and expressed as the mean ± SEM (n = 4). One sample t-test was used to analyze the significance of the obtained data separately comparing the effect of each compound with the control. Bonferroni correction of the p-value for multiple comparisons was performed (** $p < 0.01$).

Hydrogels significantly affect the amount of ROS produced by neutrophils

Once the antioxidant activity of tested hydrogels was confirmed, the effect of their presence on the detectable amount of ROS produced spontaneously by neutrophils or after their activation by OZP was tested. The oxidative burst of neutrophils is primarily characterized by the production of the superoxide anion radical, the first ROS produced by neutrophils upon their contact with a variety of stimuli (e.g., opsonins, cytokines, fragments of bacterial membranes, and others) which may appear in the wounded area.

In the case of spontaneous ROS production, the SCN/DAC_2% hydrogels slightly activate neutrophils. The greater antioxidant effect of PPy-containing compounds however manifests as ROS signal decreases depending on the amount of PPy. Although the SCN/DAC_PPy5% hydrogel reduced activation only to the level of control, the PPy10% hydrogel significantly reduced the ROS signal to 64 % of control (Figure 7a). In the case of OZP-activated ROS production, the neat SCN/DAC_2% hydrogel itself was already able to significantly reduce the ROS signal to 82% of control. The PPy5% hydrogel significantly reduced the ROS signal to 48% of the control and the PPy10 % hydrogel to 40% of the control. The antioxidant effect of PPy-containing hydrogels showed similar trends to those observed in spontaneous production, i.e. increasing with an increasing amount of PPy (Figure 7).

Regarding the role of ROS in cellular homeostasis, there is evidence to suggest that basal levels of ROS maintain normal cellular functioning and homeostasis, while significantly low levels of ROS induce cell cycle arrest. On the other hand, elevated levels induce a number of transcription factors that control the cellular defense response, and excessive ROS production activates pro-apoptotic proteins and the subsequent induction of cell death and, in extreme cases, cell necrosis. (Dunnill et al., 2017; Trachootham et al., 2008) As seen from the results, the used hydrogels, namely SCN/DAC_2% and SCN/DAC_PPy5%, could help to maintain the balance of ROS production at the site of application. For the non-activated

neutrophils, they either slightly increase or do not reduce the ROS production, thus helping to slightly stimulate neutrophils or keep a healthy amount of ROS. On the other hand, when ROS production is increased (neutrophils activated by OZP), they significantly reduce ROS production, which couold prevent negative effects on other cells and surrounding tissues (Figure 7).

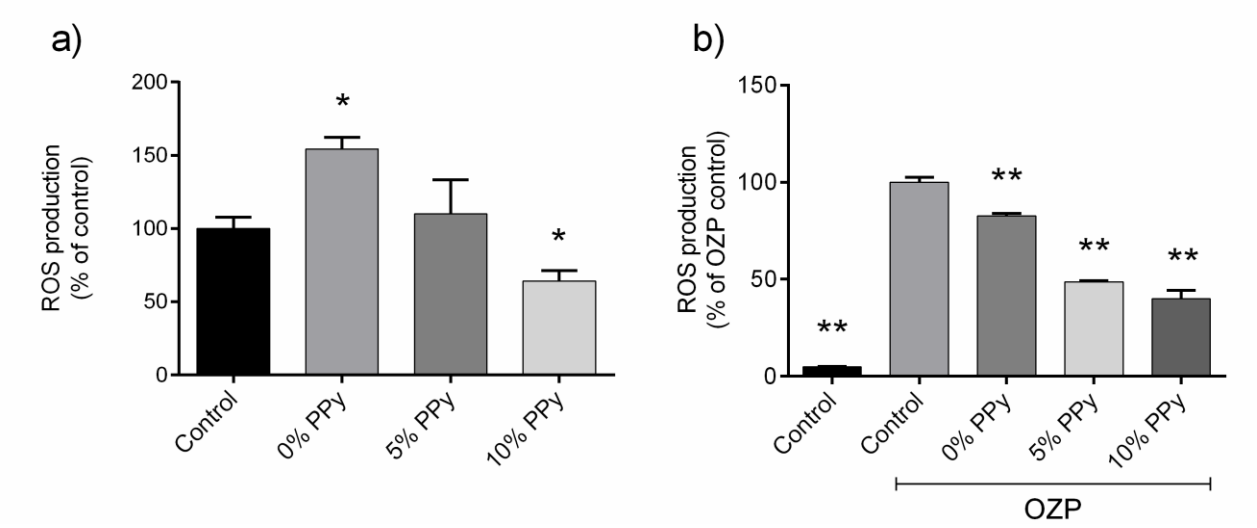

Figure 7: The effect of SCN/DAC_2% (noted as 0% PPy), SCN/DAC_PPy5% (5 % PPy), and SCN/DAC_PPy10% (10 % PPy) on spontaneous ROS production (panel a) and on OZP-activated ROS production (panel b) by neutrophils. Data were converted to a percentage of the relevant control and expressed as the mean ± SEM (n = 4). One sample t-test was used to analyze the significance of the obtained data separately comparing the effect of each compound with relevant control, i.e. ROS production of non-activated and OZP-activated neutrophils. Bonferroni correction of the p-value for multiple comparisons was performed (* $p < 0.05$, ** $p < 0.01$).

The macrophages are activated by hydrogels

Macrophages are key regulators of the wound healing process, during which they play various roles to ensure proper healing. It is well known that the phenotype of macrophages evolves with different phases of wound healing. (Krzyszczyk et al., 2018) In the initial phase of wound healing, pro-inflammatory macrophages, traditionally called “M1” macrophages, infiltrate the wound to clear it of bacteria, foreign debris, and dead cells. (Krzyszczyk et al., 2018) According to the MTT assay, the tested hydrogels had no cytotoxic effects on macrophages. On the other hand, they were able to significantly increase proliferation as seen in the mitochondrial activity (Figure 8a and 8b). Based on the results from NO and IL-6 production, it can be concluded that the tested PPy-containing hydrogels activate macrophages and thus can positively modulate the macrophage response (Figure 8c – 8f). In addition, they were able to elevate the cellular response above LPS activation, as seen in NO and IL-6 production (Figure 8d and 8f). Such increased production of mediators (particularly NO production) is needed in the acute wound healing processes. NO has been shown to modulate chemoattractant cytokines that initiate post-wound inflammation, including IL-8, and TGF-β1, and plays a key role in the angiogenesis process, affecting proliferation, differentiation, and apoptosis in many cell types involved in wound healing. (Luo & Chen, 2005)

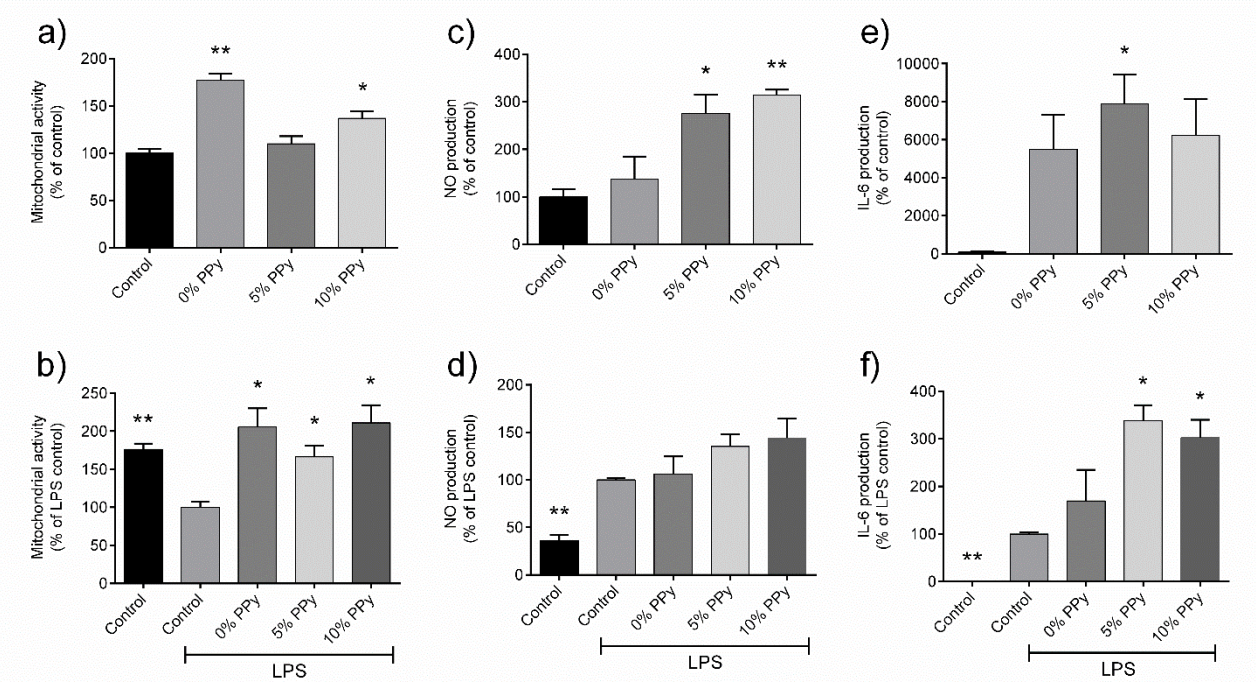

Figure 8: The effect of SCN/DAC_2% (noted as 0% PPy), SCN/DAC_PPy5% (5 % PPy), and SCN/DAC_PPy10% (10 % PPy) hydrogels on mitochondrial activity (panels a and b), NO (panels c and d), and IL-6 production (panels e and f) of RAW264.7 macrophages. Results are obtained after 24 hours without (panels a, c, and e) and after 15 ng/ml LPS activation (panels b, d, and f). Data were converted to a percentage of the relevant control and expressed as the mean ± SEM (n = 4). One sample t-test was used to analyze the significance of the obtained data separately comparing the effect of each compound with reference. Bonferroni correction of the p-value for multiple comparisons was performed (*p < 0.05; **p < 0.01).

The presence of PPy induces significant antibacterial activity

An ideal wound dressing should be antimicrobial as bacterial infections could increase the exudate formation, delay wound healing, and induce excessive and potentially chronic inflammation. (X. Zhao et al., 2017) Antibacterial wound dressings can promote wound healing by reducing the number of pathogens entering the wound, which reduces the inflammatory response. Hence, the antibacterial activity of SCN/DAC_PPy hydrogels was evaluated against *E. coli* (Gram-negative) and *S. aureus* (Gram-positive) bacteria according to standard ISO 22196 and antibacterial activity R was established (Table 1) relative to neat SCN/DAC. According to ISO 22196, an antibacterial agent can be considered effective if the R-value is >1.

Table 1: Antibacterial activity of SCN/DAC_PPy hydrogels against *E. coli* and *S. aureus*

	S. aureus	*E. coli*
SCN/DAC_2%	U_t^*= 0.061	U_t^*= 0.439
	Antimicrobial activity R	
SCN/DAC_PPy5%	2.138	0.783
SCN/DAC_PPy10%	2.072	0.989

*U_t is the average of the common logarithm of the number of viable bacteria recovered from the reference sample after 24 h.

Compared to the reference SCN/DAC hydrogel, whose antibacterial activity was low (Qin et al., 2006), the addition of PPy particles greatly improves the antibacterial activity of hydrogels, in particular against *S. aureus*, where significant antimicrobial activity was observed (R ~2.1). The antibacterial activity of PPy-containing hydrogels against *E. coli* is weaker, between 0.8 (PPy 5%) and 1.0 (PPy 10%), but the PPy 10% sample can be considered effective also against *E. coli*.

4. Conclusions

Non-cytotoxic, antibacterial, non-irritating, antioxidant, and conductive hydrogels that significantly accelerate the wound healing process *in vitro* and modulate the immune response of macrophages and neutrophils *in vitro* were prepared. They are based on partially re-acetylated chitosan (DD = 57%) which is soluble at physiological pH without any artificial modifications of the chitosan. Dialdehyde cellulose, a sustainable and low-toxic cellulose derivative serves both for crosslinking and for anchoring of pre-made polypyrrole colloidal particles, which were prepared by using low-toxicity inorganic reducing agents and which possess very low cytotoxicity themselves. The use of toxic organic compounds and crosslinkers was thus entirely avoided during the synthesis, as well as the need for an acidic environment normally required for dissolving the chitosan. The resulting SCN/DAC_PPy hydrogels are prepared by simple blending and cast-drying of the constituents. They do not require extensive washing and neutralization, which further simplifies the whole process. The condensation reaction between DAC and PPy, described here for the first time, allows not only better anchoring of PPy particles but also strengthens the hydrogel network. This provides more freedom for tuning and improving the physical properties of hydrogels, without an unnecessary increase in the amount of crosslinker. However, one should carefully select the optimal PPy: DAC ratio (here 2% of DAC and 5% of PPy relative to SCN were found optimal), otherwise a locally-dense PPy-centered network is formed, which may degrade the overall mechanical properties of hydrogels. The PPy particles are also finely dispersed in the hydrogel without the formation of aggregates, deposits, or sediments, which is a considerable advantage over the methods employing poorly controllable *in-situ* PPy polymerization or dip-coating for the preparation of conductive composite dressings and scaffolds. Prepared hydrogels also show very good skin adhesion and no irritation in full-thickness skin models.

The best overall results were obtained for the hydrogels with 2 mol.% of DAC and 5 wt.% of PPy, which showed the best mechanical properties, greatest acceleration of wound healing *in vitro*, highest antibacterial activity against *S. aureus*, specific conductivity comparable to human tissues, significant free radical scavenging capacity, modulation of ROS production by neutrophils and stimulation of NO and IL-6 production of macrophages.

To summarize, compared to neat SCN/DAC hydrogels, the synergic effect of SCN and PPy greatly improves the properties of prepared composite hydrogels in multiple areas favorable to the wound healing process, from scavenging the ROS to innate antimicrobial action. The prepared SCN/DAC_PPy5% hydrogel thus possesses numerous characteristics of the next generation of active wound dressings, however, we emphasize that further biological testing, particularly *in vivo* evaluations, is required before such application can be considered. Nevertheless, the obtained results are comparable to other reported conductive biomaterials designed for wound healing. (Yu et al., 2021) For instance, observed conductivity, antioxidative properties, and antibacterial activity are similar to those reported for conductive hydrogels based on soluble chitosan derivatives (X. Zhao et al., 2017), but without the need for artificial modifications of chitosan amine groups or the use of synthetic linkers. The SCN thus may provide a viable alternative to these soluble chitosan species when combined with PPy. The condensation reaction between DAC and PPy could also find broad applications in the field of preparation of conductive scaffolds and hydrogels in the future.

Acknowledgments

This work was supported by the Ministry of Education, Youth and Sports of the Czech Republic – DKRVO (RP/CPS/2022/001) and DKRVO (RP/CPS/2022/007). S.K. and K.V. also appreciate the support of the Internal Grants of TBU in Zlin IGA/CPS/2023/001 funded from the resources of specific academic research. The Czech Science Foundation grant 23-07425S is greatly acknowledged.

Associated Information

Supplementary Information. Supplementary Information is available: IR spectra of SCN and DAC, HSQC spectrum of SCN, rheological measurements, and biological evaluation of SCN/DAC hydrogels.

Author Information

Author Contributions. **S. Káčerová -** Investigation, Data Curation, Formal analysis, Writing – review & editing; **M. Muchová -** Investigation, Visualization, Data Curation; **H. Doudová** – Investigation; **L. Münster -** Investigation, Methodology, Writing – Original Draft; **B. Hanulíková**, Investigation, Data Curation, Visualization; **K. Valášková** – Investigation; **V. Kašpárková -** Formal analysis, Writing – review & editing; **I. Kuřitka -** Funding acquisition, Methodology; **P. Humpolíček -** Funding acquisition, Methodology, Writing – Original Draft; **Z. Víchová -** Investigation, Data Curation, Formal analysis, Writing – review & editing; **O. Vašíček -** Investigation, Methodology, Validation, Visualization, Formal analysis, Writing – Original Draft, Writing – review & editing; **J. Vícha:** Conceptualization, Investigation, Validation, Visualization, Formal analysis, Writing – Original Draft, Writing – review & editing;

Notes

The authors declare no competing financial interest.

References

Abdelgawad, A. M., Hudson, S. M., & Rojas, O. J. (2014). Antimicrobial wound dressing nanofiber mats from multicomponent (chitosan/silver-NPs/polyvinyl alcohol) systems. *Carbohydrate Polymers*, *100*, 166–178. https://doi.org/10.1016/j.carbpol.2012.12.043

Ali Khan, Z., Jamil, S., Akhtar, A., Mustehsan Bashir, M., & Yar, M. (2020). Chitosan based hybrid materials used for wound healing applications- A short review. *International Journal of Polymeric Materials and Polymeric Biomaterials*, *69*(7), 419–436. https://doi.org/10.1080/00914037.2019.1575828

Bano, I., Arshad, M., Yasin, T., Ghauri, M. A., & Younus, M. (2017). Chitosan: A potential biopolymer for wound management. *International Journal of Biological Macromolecules*, *102*, 380–383. https://doi.org/10.1016/j.ijbiomac.2017.04.047

Biswal, A., Purohit, S. S., & Swain, S. K. (2023). Chitosan based composite scaffolds in skin wound repair: A review. *Journal of Drug Delivery Science and Technology*, *84*, 104549. https://doi.org/10.1016/j.jddst.2023.104549

Bryan, N., Ahswin, H., Smart, N., Bayon, Y., Wohlert, S., & Hunt, J. A. (2012). Reactive oxygen species (ROS)—A family of fate deciding molecules pivotal in constructive inflammation and wound healing. *European Cells & Materials*, *24*, 249–265. https://doi.org/10.22203/ecm.v024a18

Das, S., & Baker, A. B. (2016). Biomaterials and Nanotherapeutics for Enhancing Skin Wound Healing. *Frontiers in Bioengineering and Biotechnology*, *4*. https://www.frontiersin.org/article/10.3389/fbioe.2016.00082

Ding, W., & Wu, Y. (2020). Sustainable dialdehyde polysaccharides as versatile building blocks for fabricating functional materials: An overview. *Carbohydrate Polymers*, *248*, 116801. https://doi.org/10.1016/j.carbpol.2020.116801

Důbravová, A., Muchová, M., Škoda, D., Lovecká, L., Šimoníková, L., Kuřitka, I., Vícha, J., & Münster, L. (2024). Highly efficient affinity anchoring of gold nanoparticles on chitosan nanofibers via

779 dialdehyde cellulose for reusable catalytic devices. *Carbohydrate Polymers*, *323*, 121435.
780 https://doi.org/10.1016/j.carbpol.2023.121435
781 Duck, F. A. (1990). Chapter 6—Electrical Properties of Tissue. In F. A. Duck (Ed.), *Physical Properties of*
782 *Tissues* (pp. 167–223). Academic Press. https://doi.org/10.1016/B978-0-12-222800-1.50010-3
783 Dunnill, C., Patton, T., Brennan, J., Barrett, J., Dryden, M., Cooke, J., Leaper, D., & Georgopoulos, N. T.
784 (2017). Reactive oxygen species (ROS) and wound healing: The functional role of ROS and
785 emerging ROS-modulating technologies for augmentation of the healing process. *International*
786 *Wound Journal*, *14*(1), 89–96. https://doi.org/10.1111/iwj.12557
787 Fan, P., Zeng, Y., Zaldivar-Silva, D., Agüero, L., & Wang, S. (2023). Chitosan-Based Hemostatic Hydrogels:
788 The Concept, Mechanism, Application, and Prospects. *Molecules*, *28*(3), 1473.
789 https://doi.org/10.3390/molecules28031473
790 Feng, P., Luo, Y., Ke, C., Qiu, H., Wang, W., Zhu, Y., Hou, R., Xu, L., & Wu, S. (2021). Chitosan-Based
791 Functional Materials for Skin Wound Repair: Mechanisms and Applications. *Frontiers in*
792 *Bioengineering and Biotechnology*, *9*.
793 https://www.frontiersin.org/articles/10.3389/fbioe.2021.650598
794 Feng, T., Du, Y., Li, J., Wei, Y., & Yao, P. (2006). Antioxidant activity of half N-acetylated water-soluble
795 chitosan in vitro. *European Food Research and Technology*, *225*(1), 133.
796 https://doi.org/10.1007/s00217-006-0391-0
797 Feng, W., & Wang, Z. (2022). Shear-thinning and self-healing chitosan-graphene oxide hydrogel for
798 hemostasis and wound healing. *Carbohydrate Polymers*, *294*, 119824.
799 https://doi.org/10.1016/j.carbpol.2022.119824
800 Feng, W., & Wang, Z. (2023). Tailoring the Swelling-Shrinkable Behavior of Hydrogels for Biomedical
801 Applications. *Advanced Science*, *10*(28), 2303326. https://doi.org/10.1002/advs.202303326

802 Flory, P. J., & Rehner, J. (1943). Statistical Mechanics of Crosslinked Polymer Networks II. Swelling. *The*
803 *Journal of Chemical Physics*, *11*(11), 521–526. https://doi.org/10.1063/1.1723792
804 Georgiev, Y. N., Paulsen, B. S., Kiyohara, H., Ciz, M., Ognyanov, M. H., Vasicek, O., Rise, F., Denev, P. N.,
805 Yamada, H., Lojek, A., Kussovski, V., Barsett, H., Krastanov, A. I., Yanakieva, I. Z., & Kratchanova,
806 M. G. (2017). The common lavender (Lavandula angustifolia Mill.) pectic polysaccharides
807 modulate phagocytic leukocytes and intestinal Peyer's patch cells. *Carbohydrate Polymers*, *174*,
808 948–959. https://doi.org/10.1016/j.carbpol.2017.07.011
809 Gizdavic-Nikolaidis, M., Travas-Sejdic, J., Bowmaker, G. A., Cooney, R. P., Thompson, C., & Kilmartin, P. A.
810 (2004). The antioxidant activity of conducting polymers in biomedical applications. *Current*
811 *Applied Physics*, *4*(2), 347–350. https://doi.org/10.1016/j.cap.2003.11.045
812 Gu, C.-Z., Feng, Y.-Q., Liu, P.-P., & Meng, S.-X. (2015). Selective synthesis of β-unsubstituted meso-aryl
813 substituted tripyrranes in water. *Journal of Saudi Chemical Society*, *19*(2), 227–232.
814 https://doi.org/10.1016/j.jscs.2014.05.004
815 Guo, S., & DiPietro, L. A. (2010). Factors Affecting Wound Healing. *Journal of Dental Research*, *89*(3),
816 219–229. https://doi.org/10.1177/0022034509359125
817 Iii, G. R. G., & S. Lindsey, J. (2001). Investigation of porphyrin -forming reactions. Part 1. Pyrrole +
818 aldehyde oligomerization in two-step, one-flask syntheses of meso-substituted porphyrins.
819 *Journal of the Chemical Society, Perkin Transactions 2*, *0*(5), 677–686.
820 https://doi.org/10.1039/B009088N
821 Jin, X., Jiang, H., Li, G., Fu, B., Bao, X., Wang, Z., & Hu, Q. (2020). Stretchable, conductive PAni-PAAm-
822 GOCS hydrogels with excellent mechanical strength, strain sensitivity and skin affinity. *Chemical*
823 *Engineering Journal*, *394*, 124901. https://doi.org/10.1016/j.cej.2020.124901

824 Káčerová, S., Víchová, Z., Valášková, K., Vícha, J., Münster, L., Kašpárková, V., Vašíček, O., & Humpolíček,
825 P. (2023). Biocompatibility of colloidal polypyrrole. *Colloids and Surfaces B: Biointerfaces*, *232*,
826 113605. https://doi.org/10.1016/j.colsurfb.2023.113605
827 Kasaai, M. R. (2010). Determination of the degree of N-acetylation for chitin and chitosan by various
828 NMR spectroscopy techniques: A review. *Carbohydrate Polymers*, *79*(4), 801–810.
829 https://doi.org/10.1016/j.carbpol.2009.10.051
830 Kim, U.-J., Kuga, S., Wada, M., Okano, T., & Kondo, T. (2000). Periodate Oxidation of Crystalline Cellulose.
831 *Biomacromolecules*, *1*(3), 488–492. https://doi.org/10.1021/bm0000337
832 Kim, U.-J., Lee, Y. R., Kang, T. H., Choi, J. W., Kimura, S., & Wada, M. (2017). Protein adsorption of
833 dialdehyde cellulose-crosslinked chitosan with high amino group contents. *Carbohydrate*
834 *Polymers*, *163*(Supplement C), 34–42. https://doi.org/10.1016/j.carbpol.2017.01.052
835 Kim, U.-J., Wada, M., & Kuga, S. (2004). Solubilization of dialdehyde cellulose by hot water. *Carbohydrate*
836 *Polymers*, *56*(1), 7–10. https://doi.org/10.1016/j.carbpol.2003.10.013
837 Korupalli, C., Li, H., Nguyen, N., Mi, F.-L., Chang, Y., Lin, Y.-J., & Sung, H.-W. (2021). Conductive Materials
838 for Healing Wounds: Their Incorporation in Electroactive Wound Dressings, Characterization, and
839 Perspectives. *Advanced Healthcare Materials*, *10*(6), 2001384.
840 https://doi.org/10.1002/adhm.202001384
841 Krzyszczyk, P., Schloss, R., Palmer, A., & Berthiaume, F. (2018). The Role of Macrophages in Acute and
842 Chronic Wound Healing and Interventions to Promote Pro-wound Healing Phenotypes. *Frontiers*
843 *in Physiology*, *9*. https://www.frontiersin.org/articles/10.3389/fphys.2018.00419
844 Kubota, N., Tatsumoto, N., Sano, T., & Toya, K. (2000). A simple preparation of half N-acetylated chitosan
845 highly soluble in water and aqueous organic solvents. *Carbohydrate Research*, *324*(4), 268–274.
846 https://doi.org/10.1016/S0008-6215(99)00263-3

847 Liang, C.-C., Park, A. Y., & Guan, J.-L. (2007). In vitro scratch assay: A convenient and inexpensive method
848 for analysis of cell migration in vitro. *Nature Protocols*, *2*(2), Article 2.
849 https://doi.org/10.1038/nprot.2007.30
850 Liang, Y., & Goh, J. C.-H. (2020). Polypyrrole-Incorporated Conducting Constructs for Tissue Engineering
851 Applications: A Review. *Bioelectricity*, *2*(2), 101–119. https://doi.org/10.1089/bioe.2020.0010
852 Luo, J., & Chen, A. F. (2005). Nitric oxide: A newly discovered function on wound healing. *Acta*
853 *Pharmacologica Sinica*, *26*(3), Article 3. https://doi.org/10.1111/j.1745-7254.2005.00058.x
854 MacNeil, S. (2007). Progress and opportunities for tissue-engineered skin. *Nature*, *445*(7130), Article
855 7130. https://doi.org/10.1038/nature05664
856 Malone-Povolny, M. J., Maloney, S. E., & Schoenfisch, M. H. (2019). Nitric Oxide Therapy for Diabetic
857 Wound Healing. *Advanced Healthcare Materials*, *8*(12), 1801210.
858 https://doi.org/10.1002/adhm.201801210
859 Matica, M. A., Aachmann, F. L., Tøndervik, A., Sletta, H., & Ostafe, V. (2019). Chitosan as a Wound
860 Dressing Starting Material: Antimicrobial Properties and Mode of Action. *International Journal of*
861 *Molecular Sciences*, *20*(23), Article 23. https://doi.org/10.3390/ijms20235889
862 Moeini, A., Pedram, P., Makvandi, P., Malinconico, M., & Gomez d'Ayala, G. (2020). Wound healing and
863 antimicrobial effect of active secondary metabolites in chitosan-based wound dressings: A
864 review. *Carbohydrate Polymers*, *233*, 115839. https://doi.org/10.1016/j.carbpol.2020.115839
865 Moosova, Z., Pekarova, M., Sindlerova, L. S., Vasicek, O., Kubala, L., Blaha, L., & Adamovsky, O. (2019).
866 Immunomodulatory effects of cyanobacterial toxin cylindrospermopsin on innate immune cells.
867 *Chemosphere*, *226*, 439–446. https://doi.org/10.1016/j.chemosphere.2019.03.143
868 Muchová, M., Münster, L., Capáková, Z., Mikulcová, V., Kuřitka, I., & Vícha, J. (2020). Design of
869 dialdehyde cellulose crosslinked poly(vinyl alcohol) hydrogels for transdermal drug delivery and

wound dressings. *Materials Science and Engineering: C*, *116*, 111242. https://doi.org/10.1016/j.msec.2020.111242

Muchová, M., Münster, L., Vávrová, A., Capáková, Z., Kuřitka, I., & Vícha, J. (2022). Comparison of dialdehyde polysaccharides as crosslinkers for hydrogels: The case of poly(vinyl alcohol). *Carbohydrate Polymers*, *279*, 119022. https://doi.org/10.1016/j.carbpol.2021.119022

Münster, L., Capáková, Z., Fišera, M., Kuřitka, I., & Vícha, J. (2019). Biocompatible dialdehyde cellulose/poly(vinyl alcohol) hydrogels with tunable properties. *Carbohydrate Polymers*, *218*, 333–342. https://doi.org/10.1016/j.carbpol.2019.04.091

Münster, L., Fojtů, M., Capáková, Z., Muchová, M., Musilová, L., Vaculovič, T., Balvan, J., Kuřitka, I., Masařík, M., & Vícha, J. (2021). Oxidized polysaccharides for anticancer-drug delivery: What is the role of structure? *Carbohydrate Polymers*, *257*, 117562. https://doi.org/10.1016/j.carbpol.2020.117562

Münster, L., Vícha, J., Klofáč, J., Masař, M., Hurajová, A., & Kuřitka, I. (2018). Dialdehyde cellulose crosslinked poly(vinyl alcohol) hydrogels: Influence of catalyst and crosslinker shelf life. *Carbohydrate Polymers*, *198*, 181–190. https://doi.org/10.1016/j.carbpol.2018.06.035

Münster, L., Vícha, J., Klofáč, J., Masař, M., Kucharczyk, P., & Kuřitka, I. (2017). Stability and aging of solubilized dialdehyde cellulose. *Cellulose*, *24*(7), 2753–2766. https://doi.org/10.1007/s10570-017-1314-x

Muthu, M., Gopal, J., Chun, S., Devadoss, A. J. P., Hasan, N., & Sivanesan, I. (2021). Crustacean Waste-Derived Chitosan: Antioxidant Properties and Future Perspective. *Antioxidants*, *10*(2), Article 2. https://doi.org/10.3390/antiox10020228

Nazarzadeh Zare, E., Mansour Lakouraj, M., & Mohseni, M. (2014). Biodegradable polypyrrole/dextrin conductive nanocomposite: Synthesis, characterization, antioxidant and antibacterial activity. *Synthetic Metals*, *187*, 9–16. https://doi.org/10.1016/j.synthmet.2013.09.045

Norahan, M. H., Pedroza-González, S. C., Sánchez-Salazar, M. G., Álvarez, M. M., & Trujillo de Santiago, G. (2022). Structural and biological engineering of 3D hydrogels for wound healing. *Bioactive Materials*, *24*, 197–235. https://doi.org/10.1016/j.bioactmat.2022.11.019

Patrulea, V., Ostafe, V., Borchard, G., & Jordan, O. (2015). Chitosan as a starting material for wound healing applications. *European Journal of Pharmaceutics and Biopharmaceutics*, *97*, 417–426. https://doi.org/10.1016/j.ejpb.2015.08.004

Peters, M. J., Stinstra, J. G., & Hendriks, M. (2001). Estimation of the electrical conductivity of human tissue. *Electromagnetics*, *21*(7–8), 545–557. Scopus. https://doi.org/10.1080/027263401752246199

Qin, C., Li, H., Xiao, Q., Liu, Y., Zhu, J., & Du, Y. (2006). Water-solubility of chitosan and its antimicrobial activity. *Carbohydrate Polymers*, *63*(3), 367–374. https://doi.org/10.1016/j.carbpol.2005.09.023

Sogias, I. A., Khutoryanskiy, V. V., & Williams, A. C. (2010). Exploring the Factors Affecting the Solubility of Chitosan in Water. *Macromolecular Chemistry and Physics*, *211*(4), 426–433. https://doi.org/10.1002/macp.200900385

Trachootham, D., Lu, W., Ogasawara, M. A., Valle, N. R.-D., & Huang, P. (2008). Redox Regulation of Cell Survival. *Antioxidants & Redox Signaling*, *10*(8), 1343–1374. https://doi.org/10.1089/ars.2007.1957

Vasicek, O., Lojek, A., Jancinova, V., Nosal, R., & Ciz, M. (2014). Role of histamine receptors in the effects of histamine on the production of reactive oxygen species by whole blood phagocytes. *Life Sciences*, *100*(1), 67–72. https://doi.org/10.1016/j.lfs.2014.01.082

Vasicek, O., Rubanova, D., Chytkova, B., & Kubala, L. (2020). Natural pseurotins inhibit proliferation and inflammatory responses through the inactivation of STAT signaling pathways in macrophages. *Food and Chemical Toxicology*, *141*, 111348. https://doi.org/10.1016/j.fct.2020.111348

Wan Yusof, W. R., Awang, N. Y. F., Azhar Laile, M. A., Azizi, J., Awang Husaini, A. A. S., Seeni, A., Wilson, L. D., & Sabar, S. (2023). Chemically modified water-soluble chitosan derivatives: Modification strategies, biological activities, and applications. *Polymer-Plastics Technology and Materials*, *62*(16), 2182–2220. https://doi.org/10.1080/25740881.2023.2249979

Wang, Q. Z., Chen, X. G., Liu, N., Wang, S. X., Liu, C. S., Meng, X. H., & Liu, C. G. (2006). Protonation constants of chitosan with different molecular weight and degree of deacetylation. *Carbohydrate Polymers*, *65*(2), 194–201. https://doi.org/10.1016/j.carbpol.2006.01.001

Yu, R., Zhang, H., & Guo, B. (2021). Conductive Biomaterials as Bioactive Wound Dressing for Wound Healing and Skin Tissue Engineering. *Nano-Micro Letters*, *14*, 1. https://doi.org/10.1007/s40820-021-00751-y

Zhao, W., Wang, Y., & Wang, A. (2017). Nonlinear Optical Properties of Novel Polypyrrole Derivatives Bearing Different Aromatic Segments. *Materials Sciences and Applications*, *8*(11), Article 11. https://doi.org/10.4236/msa.2017.811056

Zhao, X., Wu, H., Guo, B., Dong, R., Qiu, Y., & Ma, P. X. (2017). Antibacterial anti-oxidant electroactive injectable hydrogel as self-healing wound dressing with hemostasis and adhesiveness for cutaneous wound healing. *Biomaterials*, *122*, 34–47. https://doi.org/10.1016/j.biomaterials.2017.01.011